U.S. Department of Energy
Energy Efficiency and Renewable Energy
Bringing you a prosperous future where energy is clean, abundant, reliable, and affordable

Industrial Technologies Program
Industrial Materials for the Future

Final Technical Report

Development of Stronger and More Reliable Cast Austenitic Stainless Steels (H-Series) Based on Scientific Design Methodology

June 2006

Principal Investigators:

Roman I. Pankiw
Duraloy Technologies, Inc.

G. (Murali) Muralidharan and Vinod K. Sikka
Oak Ridge National Laboratory

Duraloy Technologies, Inc.

Oak Ridge National Laboratory

Managed by
UT-Battelle, LLC

ORNL/TM-2006/45

FINAL TECHNICAL REPORT

Project Title:	Development of Stronger and More Reliable Cast Austenitic Stainless Steels (H-Series) Based on Scientific Design Methodology
Award No.:	DE-FC36-01ID14245
Project Period:	09/01/2001–09/30/2005
PIs:	Mr. Roman I. Pankiw (724) 887-5100 ext. 188 techmgr@duraloy.com Dr. G. (Murali) Muralidharan (865) 574-4812 muralidhargn@ornl.gov Dr. Vinod K. Sikka (ORNL) (865) 574-5112 sikkavk@ornl.gov
Additional Researchers:	Dr. Philip J. Maziasz (ORNL)
Recipient:	Duraloy Technologies, Inc. 120 Bridge Street Scottdale, PA 15683-0081
National Laboratory:	Oak Ridge National Laboratory (ORNL) One Bethel Valley Road P.O. Box 2008 Oak Ridge, TN 37831
Industrial Partners:	Mittal Steel USA (Formerly ISG) The Timken Company EIO Harper International IPSCO Nucor Steel

ORNL/TM-2006/45

Development of Stronger and More Reliable Cast Austenitic Stainless Steels (H-Series) Based on Scientific Design Methodology

Roman I. Pankiw
Duraloy Technologies, Inc.

G. (Murali) Muralidharan and Vinod K. Sikka
Oak Ridge National Laboratory

June 2006

Prepared jointly by

Duraloy Technologies, Inc.
120 Bridge Street
Scottdale, PA 15683-0081

and

OAK RIDGE NATIONAL LABORATORY
P.O. Box 2008
Oak Ridge, Tennessee 37831-6283
managed by
UT-Battelle, LLC
for the
U.S. DEPARTMENT OF ENERGY
under contract DE-AC05-00OR22725

Acknowledgments and Disclaimer

Acknowledgments

This report is based upon work supported by the U.S. Department of Energy, Energy Efficiency and Renewable Energy, Industrial Technologies Program, Industrial Materials for the Future, under Award No. DE-FC36-01ID14245.

Research at the Oak Ridge National Laboratory was sponsored by the U.S. Department of Energy, Office of Energy Efficiency and Renewable energy, Industrial Technologies Program, under contract DE-AC05-00OR22725 with UT-Battelle, LLC. The authors wish to thank Dr. Peter Angelini for program management during the project and reviewing the document, Millie Atchley for preparation of the document, and Carolyn Moser for technical editing.

Contents

List of Figures

List of Tables

Abbreviations and Acronyms

ASM	ASM International (American Society for Materials)
ASME	American Society of Mechanical Engineers
ASTM	American Society for Testing and Materials
COST	European Cost Program
DOE	U.S. Department of Energy
EIO	Energy Industries of Ohio
HK	Trade name for Fe-25Cr-25Ni cast stainless steels
HP	Trade name for Fe-25Cr-35Ni cast stainless steels
IMF	Industrial Materials of the Future
IPSCO	IPSCO Enterprises Inc. (steel company)
ITP	Industrial Technologies Program
NRIM	National Research Institute of Metals (Japan)
ORNL	Oak Ridge National Laboratory
R&D	research and development
scf	standard cubic foot
SEM	scanning electron microscope/microscopy
UT-A	University of Texas—Arlington

1. Executive Summary

1.1 Purpose

The goal of this project was to increase the high-temperature strength of the H-Series of cast austenitic stainless steels by 50% and the upper use temperature by 86 to 140°F (30 to 60°C). Meeting this goal is expected to result in energy savings of 35 trillion Btu/year by 2020 and energy cost savings of approximately $230 million/year.

The higher-strength H-Series cast stainless steels (HK and HP type) have applications for the production of ethylene in the chemical industry, for radiant burner tubes and transfer rolls for secondary processing of steel in the steel industry, and for many applications in the heat treating industry, including radiant burner tubes.

The project was led by Duraloy Technologies, Inc., with research participation by Oak Ridge National Laboratory (ORNL) and industrial participation by a diverse group of companies. The project management and coordination plan is shown in Fig. 1.1. A related project at the University of Texas-Arlington (UT-A) is described in *Development of Semi-Stochastic Algorithm for Optimizing Alloy Composition of High-Temperature Austenitic Stainless Steels (H-Series) for Desired Mechanical and Corrosion Properties* (ORNL/TM-2005/81/R1). The final report on another related project at the University of Tennessee, by George Pharr, Easo George, and Michael Santella, has been published as *Development of Combinatorial Methods for Alloy Design and Optimization* (ORNL/TM-2005-133).

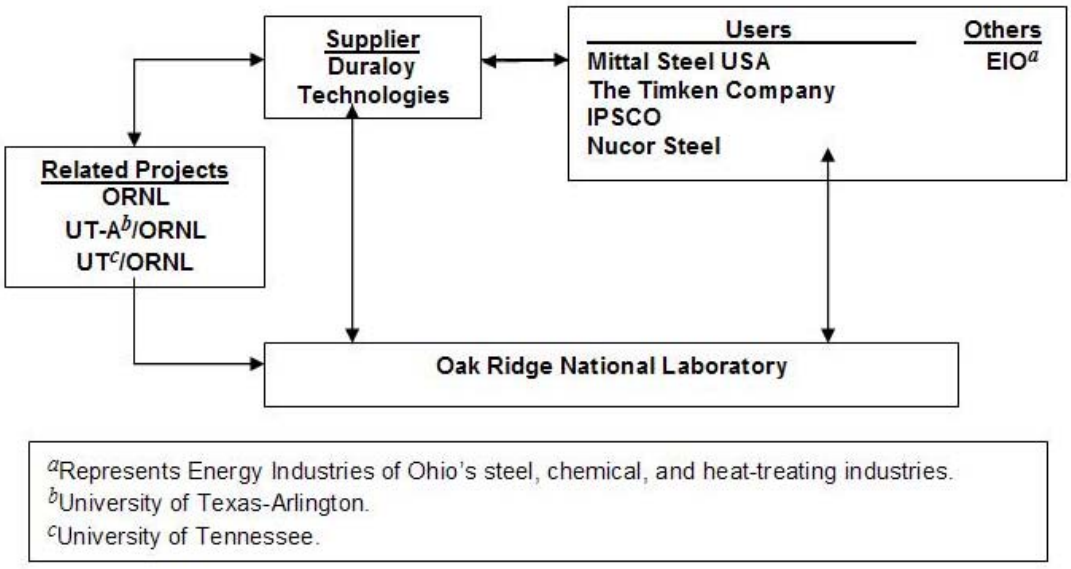

Fig. 1.1. Organization plan for project coordination and management.

The goal of the project was achieved by using the alloy design methods developed at ORNL, based on precise microcharacterization and identification of critical microstructure/properties relationships and combining them with modern computational science–based tools that calculate phases, phase fractions, and phase compositions based on alloy compositions. The combined approach of using microcharacterization of phases and computational phase prediction would permit rapid improvement in the current composition of an alloy and provide the long-term benefit of customizing alloys within grades for specific applications.

The project was appropriate for the domestic industry because the current H-Series alloys have reached their limits both in high-temperature-strength properties and in upper use temperature. The great desire of Duraloy's industrial customers to improve process energy efficiency while reducing cost requires that the current alloys be taken to the next level of strength and that the upper use temperature limit be increased.

This project addressed a specific topic from the subject call: to develop materials for manufacturing processes that will increase high-temperature strength, fatigue resistance, corrosion, and wear resistance. The outcome of the project can benefit manufacturing processes in the chemical, steel, and heat-treating industries.

1.2 Scope

The project goals were achieved through a unique approach consisting of the following steps:

1. Conduct computational thermodynamic and kinetic modeling to identify the phases in cast compositions of HK and HP steels (Fe-25Cr-25Ni and Fe-25-35Ni) as a function of temperature.
2. Conduct microstructural characterization of phases present in HK and HP steels and compare results with calculated values to radiate the output of computational models.
3. Develop correlations between creep properties and weight percentage of phases in commercially used compositions of HK and HP steels.
4. Based on correlation of creep properties, identify weight percentage of phases required to meet the project objective.
5. Use computational thermodynamic modeling to identify new compositions of HK and HP steels that are expected to meet the creep strength requirements.
6. Produce experimental size heats of newly identified compositions of HK and HP steels.
7. Conduct creep tests on new compositions to validate the predicted creep properties.
8. Produce radiant burner tubes of newly identified compositions of HP alloy and test their performance in production furnace environments.

1.3 Results

The most important result from this project was the development of a computational method for designing a high-strength low-cost version of the standard grades of cast austenitic stainless steels known as HK and HP steels. The computational models were validated in three ways: (1) through microstructural phase analysis, (2) by use of creep testing, and (3) through production and testing of radiant burner tubes in production furnace environments.

1.4 Conclusions

The computational model developed during this project provides the opportunity not only to design HK and HP steel compositions that meet the strength and upper use temperature requirements of industry but also to select lower-cost alloying elements that produce less or none of the embrittling phases during application. The results of the project can give the United States a new lead in producing higher-strength H-Series stainless steels with very significant savings of energy and associated cost savings.

1.5 Recommendations

This project accomplished all of the planned goals. However, the following steps are recommended to take further advantage of this project:

1. Creep data are the limiting factors in use of these steels for very-high-temperature industrial applications. These data are needed in the test temperature range of 1,650 to 2,200°F (900 to 1,204°C) and for test times exceeding 10,000 h and for three to five different heats of a specified composition.
2. This project has developed the higher-strength versions of HK and HP steels. However, they will still be welded by the lower-strength-version weld filler wire. The computational approach developed for base metal in this project should also be extended to develop new weld filler compositions that match or exceed the strengths of the base metal compositions.
3. For some high-risk applications, such as replacing water-cooled rolls with uncooled rolls, there is a need for U.S. Department of Energy (DOE) funding to minimize the use risk. However, if successful, such applications could produce additional energy savings.
4. No corrosion data were developed for the newly developed steels in this project. There is a need to generate data in oxidizing, carburizing, and sulfidizing environments as part of a database / knowledge base effort.

1.6 Commercialization

The progress made toward the commercialization include the following:

1. A data sheet comparing the creep properties of the newly developed HK and HP grades with currently used alloys was prepared and sent to the industrial users of HK and HP grade steels.
2. Radiant burner tube assemblies of the newly developed HP grades were produced and installed at Nucor Steel, Crawfordsville, Indiana. The tubes have operated successfully for nearly 12 months. Based on this experience, Nucor has ordered additional radiant burner tube assemblies.
3. Based on the data sheet, Nucor plants in Indiana and Alabama have shown strong interest in installing uncooled rolls in their thin-slab reheating furnaces to replace water-cooled rolls. Similar interest has been shown by Steel Dynamics. A proposal requesting DOE funding for uncooled roll application for the new HP grades was submitted to DOE's Industrial Technologies Program (ITP) during October 2005.
4. Air Products has shown a strong interest in using the new high-strength HP grade in furnace tubes for its hydrogen-cracking furnaces.
5. Duraloy is discussing the use of these alloys for other applications with additional customers. Because Duraloy is a commercial producer of HK and HP grades, it is relatively easy for the

company to introduce the newly developed steels to industrial customers as higher-performance materials.

It should be noted that the newly developed grades of HK and HP are no more expensive than the standard grades. Furthermore, they have strength and creep properties exceeding those of Supertherm™, but are free of expensive cobalt additions. In addition, the newly developed grades exhibit weldability similar to that of the currently used grades while also having greater creep strength values .

2. Introduction

2.1 Project Overview and Goals

The goal of this project was to increase the high-temperature strength of the H-Series of cast austenitic stainless steels by 50% and the upper use temperature by 86 to 140°F (30 to 60°C). Meeting this goal is expected to result in energy savings of 38 trillion Btu/year by 2020 and energy cost savings of $185 million/year.

The higher-strength H-Series cast stainless steels (HK and HP type) have applications for the production of ethylene in the chemical industry, for radiant burner tubes and transfer rolls for secondary processing of steel in the steel industry, and for many applications in the heat treating industry, including radiant burner tubes.

The mission of DOE-ITP is to help U.S. industry in becoming more energy-efficient. Among the industries identified by DOE-ITP are aluminum, steel, chemical, petrochemical, metal casting, heat treating, and forging. In many cases, energy is wasted because of a lack of continued long-term availability of the manufacturing equipment (for example, because of inadvertent shutdowns and restarts). In some cases, water-cooled components are needed to carry out a process. There are also some operations where energy efficiency can be improved if operations can be carried out at higher temperatures. A major source of energy inefficiencies in manufacturing is the inability of current materials to perform under commercial manufacturing conditions, either because they cannot withstand long production runs or because they require use of water cooling. This project addressed the very important need of developing materials that would nearly double the creep strength of current alloys and increase their maximum operating temperature by 86 to 140°F (30 to 60°C), thus increasing process energy efficiency.

The project was led by Duraloy Technologies with participation by ORNL and several potential user companies. Energy Industries of Ohio (EIO) was also a partner in this project. Each team partner had well-defined roles. Duraloy Technologies led the team by identifying the base alloys that were to be improved from this research. Duraloy also provided an extensive creep database on current alloys, provided creep-tested specimens of certain commercial alloys, and carried out centrifugal casting and component fabrication of newly designed alloys. Nucor Steel was the first partner company to install a radiant burner tube assembly in its heat-treating furnaces. Other steel companies participated in project review meetings and are currently working with Duraloy to obtain commercial components of the new alloys. EIO is promoting the enhanced performance of the newly designed alloys to Ohio-based companies, including the Timken Company.

Heat-resistant cast austenitic stainless steels, and alloys are commonly used as construction materials for process equipment in the chemical, petrochemical, heat-treating, and metals processing industries. All these applications are continuing to drive performance, durability, and use temperatures higher, while economics tries to force the cost of such alloys lower. For service temperatures above 1560–1650ºF (850–900ºC), the dominant alloys are HK-40 stainless steels or the modified or microalloyed HP stainless alloys [1–4].* Fairly complete descriptions of the properties, compositions, and standard industrial practice for the various grades of cast austenitic stainless steels and alloys can be found in handbooks or data available from the Steel Founders Society of America, the American Society for Materials (ASM) International, the Nickel Development Institute, the Specialty Steel Industry of

* The classifications used today were introduced by the Alloy Casting Institute in 1941. Heat-resistant grades are designated as H-grades; corrosion-resistant stainless steels and alloys are designated as C-grades [Ref. 1].

North America, or data sheets compiled by the various leading alloy casters. HK-40 stainless steel is essentially a Fe-25Cr-20Ni-0.4C alloy, while the HP-40 stainless alloy is Fe-25Cr-35Ni-0.4C, with more creep-resistant modifications being the HP modified (+Nb) or the HP micro-alloyed (+Nb+Ti or +Nb+Zr) materials. In the 1960s and 1970s, efforts to improve the carburization resistance of the HK-40 steels led to additions of up to 2% silicon and increases in nickel (IN-519, 25Cr-25Ni-1.5Nb and HP alloys), while efforts to increase strength and creep resistance led to the addition of niobium [1,4]. Costly upgrades of the modified HP alloys include additions of tungsten and cobalt to further increase high-temperature strength.

The basic HK alloy grade was developed and defined prior to 1940, and applications of such cast alloys to replace wrought austenitic stainless steels in ethylene furnaces or metals processing equipment was done in the 1960s. The efforts to improve the high-temperature limits or performance of HK-40 (particularly improved carburization resistance) that produced the modified or micro-alloyed HP alloys in use today occurred mainly in the late 1960s and the 1970s. Because the base technology in the United States was mature, few or no systematic or scientific studies were funded by government agencies through the 1980s and 1990s. Demand for high-performance cast alloys was static in the early to mid-1980s and then increased in the 1990s. Advanced end-use technology, particularly for petrochemical and chemical furnace tubes, has advanced by redesign of furnace tubing or by selection of premium-grade HP alloys that include cobalt or tungsten. Proprietary grades of alloys are customized by vendors to meet specific end-user requirements. Code groups [the American Society for Testing and Materials (ASTM) or the American Society of Mechanical Engineers (ASME)] provide standards for alloy grades and for critical pressure boundary applications, but many materials processing applications are not specifically covered by these codes. In the 1990s the emerging technologies involved the development and testing of advanced materials like nickel aluminides, ceramics, or other intermetallic alloys (i.e., silicides) rather than alloy development to improve existing materials such as H-Series steels.

The research and development (R&D) carried out during this project is the first of its kind to have used a computational methodology to design new compositions of HK and HP grades that

- are stronger in creep by nearly an order of magnitude than the standard HK and HP grades and
- are alloyed with lower-cost elements.

2.2 Potential Applications and Energy Savings

All of the applications where HK and HP grades are currently used can be replaced by the higher-strength versions of the same grades developed during this project. The newly developed HP grade can also replace Supertherm, a commercial higher-strength version of the HP grade that contains upt to 15 wt % of expensive elements such as cobalt and nickel.

The most significant applications for the newly developed HK and HP grades are expected to occur in three industries: chemicals, steel, and heat-treating. A summary of applications in these industries is provided below.

2.2.1 Chemical Industry: Furnace Tubes for Hydrogen Reforming Applications

According to information from Air Products and Duraloy,* an increase of 40ºF (25ºC) in hydrogen reforming furnace tubes results in 3 Btu of natural gas savings per standard cubic foot (scf) of hydrogen produced. The United States uses ~9×10^6 tons of hydrogen/year that is produced by the steam reforming process, † an amount that converts to 3.23×10^{12} scf of hydrogen. Thus, the potential energy savings in natural gas would be approximately **9.7 trillion Btu/year** just from this one process in the chemical industry.

2.2.2 Steel Industry: Steel Reheating Furnaces

The high-strength HP grade steel could replace water-cooled transfer rolls that are currently used for reheating steel thin-slab castings for in-line hot-rolling. The thin-slab casting and its on-line hot rolling requires that the steel slab exiting the continuous caster be reheated to desired temperatures at rates corresponding to the rates at which the slab is moving. To achieve such rates, reheating or tunnel furnaces are designed to deliver high heat fluxes by operating at very high temperatures. Inside the furnaces there are typically up to 100 rolls that support the slab while it moves through the furnace. Because high-strength materials are not currently available, the furnace rolls are water-cooled, a process that requires a complex roll design. Even more natural gas consumption occurs because of the need for additional heat to offset the natural furnace cooling created by the water-cooled design (made even worse as refractory thermal insulation fails).

Uncooled rolls, on the other hand, stabilize at furnace temperature. Nucor Steel, Crawfordsville, Indiana, documented a 25% decrease in gas consumption upon installation of the first 60 uncooled rolls that replaced water-cooled rolls (from 0.5 million Btu per ton of steel to 0.375 million Btu per ton of steel).‡ Furnace operating temperatures for certain regions of the furnace are so high that even newly designed higher-strength alloys would not be capable of operating in the uncooled condition. Rolls manufactured from the high-strength H-series steel composition developed in this project, based on computational alloy design, will permit the replacement of 80 of the 100 rolls in a steel reheating furnace; the energy use for the uncooled rolls will be $0.5 – (0.5–0.375) \times 80/60 = 0.333$ million Btu per ton of steel. This results in an energy savings of $0.5 – 0.333 = 0.167$ million Btu per ton of steel.

Table 2.1 lists all of the steel mills in the United States that have tunnel furnaces with water-cooled rolls, the number of furnaces (lines) that each mill has, and the steel tonnage produced by each of the mills. Based on an estimated energy savings of 0.167 million Btu per ton of steel, these mills could deliver energy savings of **2.5 trillion Btu/year** (14.75 million tons/year × 0.167 million Btu/ton).

In addition to these energy savings, there is a possibility of significant savings in the electric energy that is used to deliver the water for the cooling of rolls. The energy savings will come from the elimination of pumps, motors, valves, and heat exchangers or cooling towers.

2.2.3 Heat-Treating Industry: Radiant Burner Tubes

The major applications of the newly developed HP steels in the heat-treating industry are for radiant burner tubes. The higher strength of the HP steels developed in this project will allow higher operating temperature for the radiant burner tubes with increased heat flux and thus higher heating efficiency. Heat-treating facilities in the United States operate roughly 55,000 furnaces, 66% of which

*E-mail communication from John Hoffman of Air Products and Chemicals, Inc., and Don Voke of Duraloy Technology, Inc., Oct. 25, 2005.

†"Today's Hydrogen Production Industry," http://www.fe.doe.gov/programs/fuels/hydrogen/current technology.html.

‡ E-mail communication, "Dry Tunnel Furnace Rolls," from Dan Miller, Duraloy Technologies, Sept. 26, 2005.

Table 2.1. U.S. steel plants that use tunnel furnaces with water-cooled rolls

Steel plant	Location	Number of lines	Capacity (million tons)
ACME	Chicago, Illinois	1	1.6
BHP—Northstar	Delta, Ohio	1	1.5
Gallatin	Ghent, Kentucky	2	2.0
Nucor-Berkeley	Huger, South Carolina	2	2.0
Nucor-Crawfordsville	Crawfordsville, Indiana	2	2.0
Nucor-Decatur	Decatur, Alabama	2	2.0
Nucor-Hickman	Armorel, Arkansas	2	2.0
Steel Dynamics	Fort Wayne, Indiana	2	2.0
Total tonnage			**14.8**

are gas-fired and 33% are electrically heated.* These furnaces use a total of 458 trillion Btu of energy per year; of this amount 337 trillion Btu is natural gas, and 121 trillion Btu is electricity.

A higher-strength radiant burner tube would increase energy savings in two ways: (1) a higher operating temperature will increase heat flux and thus heating efficiency; (2) the radiant burner tubes would be longer-lived because of their higher creep strength. A conservative estimate of a 5% savings in energy through the use of radiant burner tubes made of the new HP steels would result in a natural gas energy savings of approximately 5% of 337 trillion Btu/year, or **16.8 trillion Btu/year,** and an electricity energy savings of **6.1 trillion Btu/year.**

Energy savings are also anticipated through the following:

1. The use of the higher-strength HP grade steel in ethylene furnace applications, which would enable the possibility for higher operating temperatures. To minimize coking, the inner surface of a tube would need to be lined with an anti-coking material such as the ORNL-developed alloy 4 or a weld overlay with aluminum.
2. The use of HK and HP grades for plate transfer rolls in certain steel austenitizing furnaces.
3. The use of higher-strength HP grade steels for trays and fixtures for carburizing furnaces.

Based on this discussion, a total energy savings of about 35 trillion Btu/year could be achievable between 2015 and 2020.

*_Energy and Environmental Profile_, prepared for the U.S. Department of Energy, Industrial Technologies Program, by Energetics, Inc., Oct. 2003.

3. Background and Technical Approach

3.1 Background

Japanese and European researchers made some efforts toward a better understanding of the behavior of existing cast austenitic stainless alloys and developed improved alloys in the late 1980s and through the 1990s; however, such experimental alloys were not widely adopted for commercial use. In the late 1990s, the Japanese and European governments [mainly through Japan's National Research Institute of Metals (NRIM) and the European COST Program] initiated large research efforts aimed at helping industry improve existing metals and alloys. The Japanese in particular devoted large efforts to provide databases on extremely long-term aging or service exposure of stainless steels and alloys and nickel-based superalloys (>100,000 h) to enable computational science (thermodynamic or microstructural modeling) to provide a more scientific basis for designing new alloys.

Alloy development for complex engineering alloys based on single or multiple alloying element additions or changes over wide ranges can often be very labor-intensive, time-consuming, and costly. Usually such traditional brute-force efforts produce only modest, incremental improvements, and then such improvements must be further verified by a testing regime that is relevant to real-time component service. Therefore, most applications engineers attempt to redesign components or to solve their materials problems by selecting alternate materials, and they only turn to traditional alloy development as a last resort. In the mid-1980s, a far more scientific and practical method of precise microstructural analysis and identification of the degradation/failure mechanisms was devised at ORNL to improve the creep resistance of 300-series austenitic stainless steels at 1300–1470°F (700– 800°C) [5,6]. This method provided a framework for translating the effects of various single or combined alloying elements directly into their effects on precipitation behavior or the stability of the parent matrix phase (austenite).

The native microstructure in fully austenitic HK-40 and HP alloys consists of dendritic structures of austenite matrix with finer dispersions of carbides (Cr-rich $M_{23}C_6$ or Nb-rich MC, depending on the alloy), heavier clusters of NbC in the interdendritic regions (the last liquid to solidify), and dispersions of $M_{23}C_6$ along the seams between colonies of dendrites (dendrite cores in a given colony are all parallel to <100>). Aging effects can vary, with few deleterious effects above 1740–1830°F (950–1000°C), particularly in the modified HP alloys, but with potential embrittlement (severe ductility loss at ambient temperatures) due to $M_{23}C_6$ films and/or sigma phase formation during prolonged exposure below 1650°F (900°C), mainly in the HK-40 type alloy. Additions of cobalt are made mainly to strengthen and stabilize the austenite matrix phase, while additions of tungsten promote solid solution strengthening as well as WC formation. Figure 3.1 shows the rupture strength of these various alloys as a function of temperature typical of applications used as tubing in ethylene pyrolysis furnaces. Ethylene cracking and radiant furnace tubes generally have prolonged exposure to relatively steady temperatures; under these circumstances creep resistance and oxidation/corrosion resistance are the life-defining properties. However, when such alloys (mainly HK-40) are used for materials processing applications—e.g., for the coiling drums of Steckel Mills and for calcining retorts—their required properties must go beyond creep strength and must also include thermal fatigue resistance to prevent surface cracking (critical for coiling drums) or catastrophic through-section fracture (for retorts). While it is possible to use the more expensive chemical/petrochemical premium alloys for such materials processing equipment applications, the materials processing

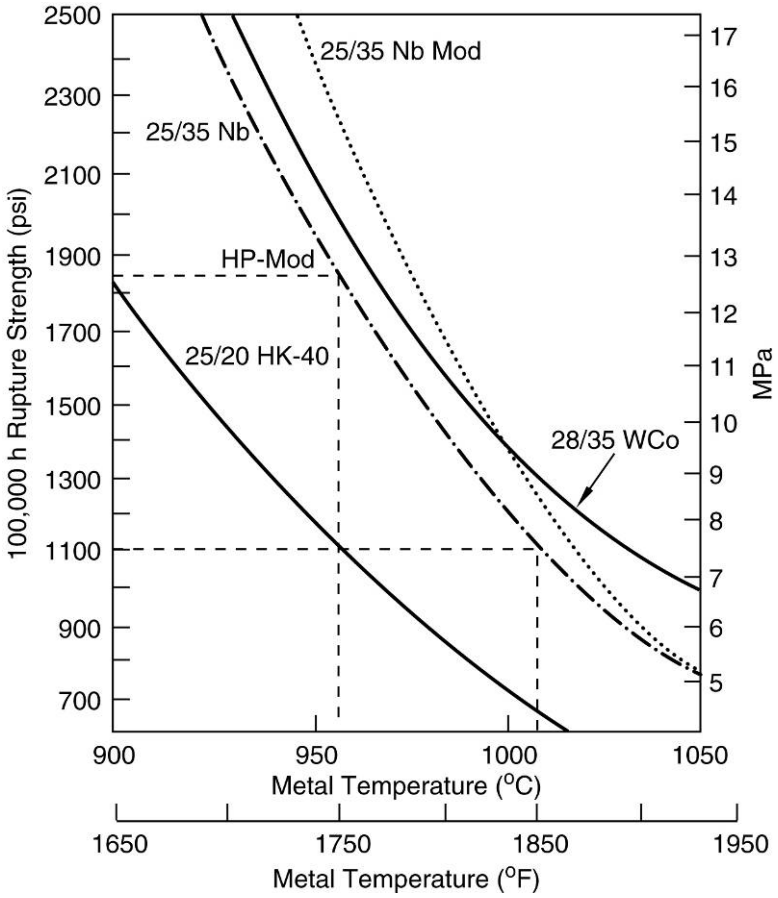

Fig. 3.1. Rupture strength of various current H-Series steel modifications as a function of temperature.

industries would probably be better served by improving the strength and aging resistance of the standard HK-40 grade steel to provide a more cost-effective solution.

At ORNL, when this scientific knowledge of how to stabilize desirable phases and reduce or eliminate undesirable phases was coupled with a thorough knowledge of microstructure/properties relationships and failure mechanism, precise microstructures were designed that produced outstanding long-term creep-resistance the first time those modified stainless steels and alloys were made [7,8]. The effects caused by alloy additions were classified as follows:

(a) direct reactant effects (i.e., Nb + C = NbC);
(b) catalytic effects (i.e., solutes that enhance the formation of a phase even though they are not direct reactants, such as silicon enhancing the formation of the Fe_2Mo Laves phase or boron enhancing the formation of TiC or $M_{23}C_6$ carbides);
(c) inhibitor effects (i.e., solutes that retard or prevent the formation of particular precipitate phases, such as C, B, and P retarding or preventing the formation of intermetallic phases like sigma, chi, or Laves); and
(d) interference effects (i.e., two or more phases competing for the same element to decouple or simplify phase behavior and control in complex alloys).

A number of microstructural effects had to be controlled to create extremely long-term creep-rupture resistance. Challenges facing researchers included

- eliminating creep voids,
- promoting fine dispersions of MC carbides,
- preventing the dissolution or coarsening of fine MC carbides,
- delaying or preventing the formation of embrittling grain-boundary intermetallic phases, and
- preventing dislocation recovery or recrystallization (mainly for wrought alloys).

The ORNL alloy design methodology produced modified type 316 austenitic stainless steels and modified 800H austenitic stainless alloys for heat-exchanger tubing applications in fossil power plants that clearly outperformed the best commercially available, comparable alloys [9]. This alloy design method was recently adapted to produce a modified 803 austenitic stainless alloy with improved creep-rupture resistance at 1500°F (816°C) [9].

In a project funded by Caterpillar, ORNL recently applied this alloy development method to developing cast austenitic stainless steels with improved creep resistance at 1300–1650°F (700–900°C) for critical exhaust component applications (manifolds and turbocharger casings) in advanced diesel engines [10–11]. Figure 3.2 shows the enhanced creep performance for new alloys compared with that of the commercial cast alloy CF-8C. The Caterpillar project clearly demonstrated that focused, meaningful alloy development can be accomplished in 1.5–2.5 years, in contrast to the traditional methods, and formed the background and basis for the current project.

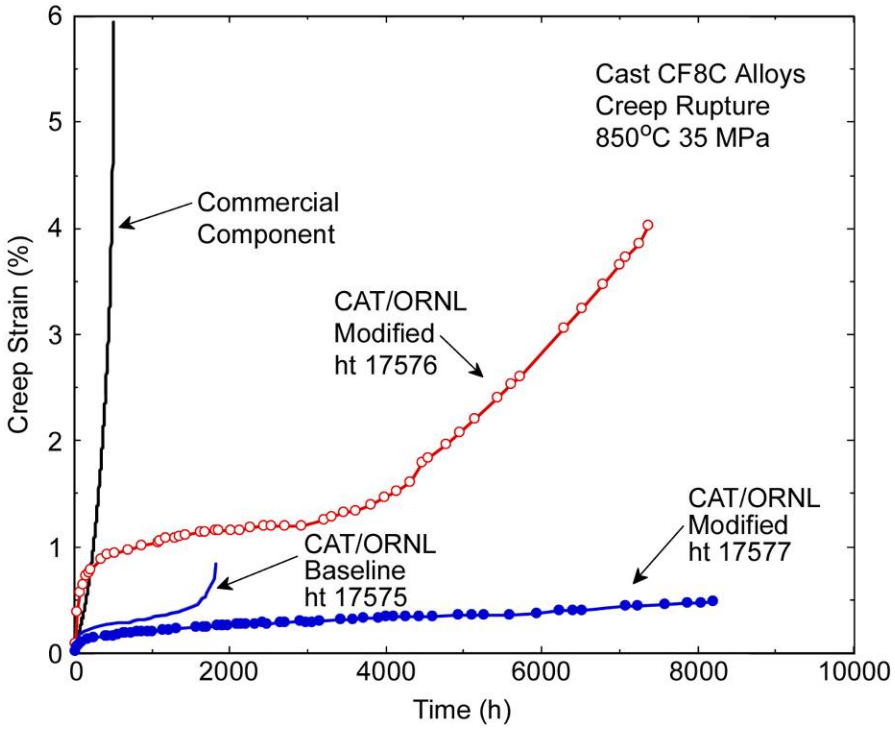

Fig. 3.2. Comparison of creep strain vs time for standard commercial and modified cast CF8C (Fe-19Cr-12Ni-Nb,C) austenitic stainless steel. Nearly an order of magnitude improvement in creep strength was achieved.

3.2 Technical Approach

In the current project, the prior approach was taken much further by adding computational capabilities to identify microstructural evolution at operating temperature as a function of time. This project was aimed at addressing the issues described above. More specifically, the goal of the project was to increase the high-temperature strength of H-Series cast austenitic steels by 50% and the upper use temperature by 86–140°F (30–60°C) through computational alloy design and microstructural characterization.

The overall project approach is illustrated in the diagram shown in Fig. 3.3. In the first phase of the project, results on phase stability and volume fraction of phases obtained through thermodynamic and kinetic modeling were compared with the actual microstructure observed through microstructural characterization of selected existing H-series alloys [12–16]. The alloys selected for this study represented a wide range in creep properties. Correlations between the microstructure and creep properties were established in this phase. Using these correlations, the microstructures required to achieve alloys with improved properties were identified, and the criteria for such microstructures were established.

In the second phase of the research, thermodynamic calculations were used to sample composition space and identify alloy compositions that would satisfy the desired microstructure criteria. Alloys with compositions that might have improved properties were prepared on the laboratory scale, and their creep properties were measured. Information obtained from the microstructure-property correlation was used to refine the existing relationships, and a new generation of alloys was identified. Alloy compositions with improved properties were identified in this work and are outlined later in the report.

Table 3.1 is a lists of the tasks that were performed over the three-year project period:

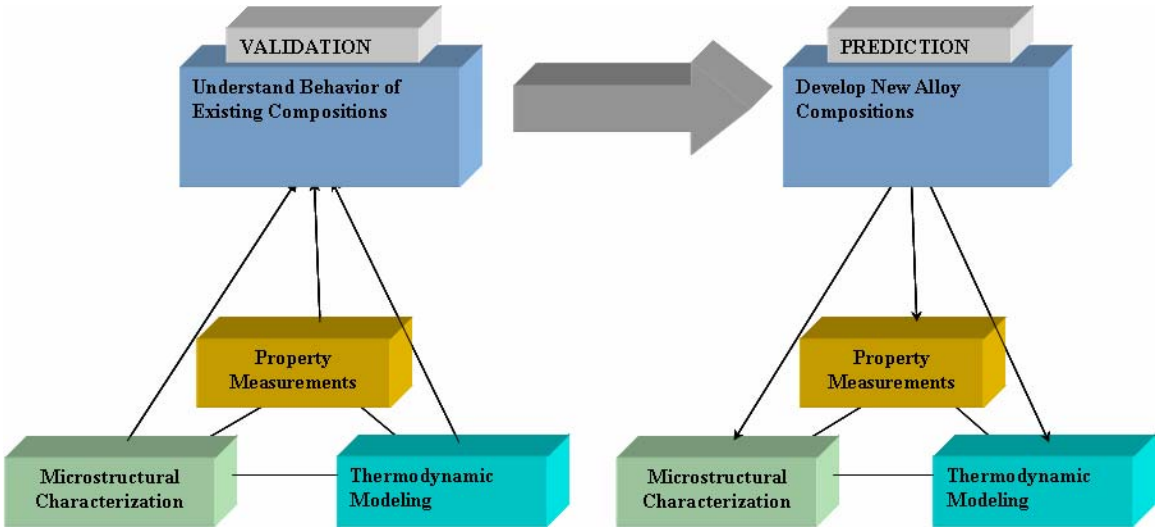

Fig. 3.3. Schematic of the overall approach adopted in this project.

Table 3.1. Work breakdown structure

ID	Task	Year 1	Year 2	Year 3
1	**Computational Thermodynamic Analysis of Various Phases in HK and HP Modified Steel**			
	1.1 ThermoCalc™ analysis of phases for current HK and HP modified compositions in the cast, aged, and removed from service conditions			
	1.2 ThermoCalc™ analysis of newly identified modifications of HK and HP modified compositions in the cast and aged conditions			
	1.3 Refining the ThermoCalc™ analysis to incorporate the cooling rates observed during the centrifugal and static castings			
2	**Micro-characterization of Specimens of HK and HP Modified for Verification of Computational Models and Correlation with Mechanical Properties**			
	2.1 Micro-characterization analysis for current HK and HP modified compositions in the cast, aged, and removed from service conditions			
	2.2 Correlate the microstructural analysis with mechanical properties			
	2.3 Identify new compositions of improved strength and thermal stability based on verified computational analysis and microstructural/mechanical property correlation			
3	**Cast Experimental Size Heats of New Compositions Developed Based on Tasks 1 and 2 and Determine Their Mechanical Properties**			
	3.1 Melt 20-lb-size heats and cast into 1 × 4 × 6-in. slabs			
	3.2 Conduct stress relaxation tests on cast compositions			
	3.3 Conduct detailed mechanical properties testing of selected compositions			
	3.4 Correlate mechanical properties with microstructure			
4	**Centrifugal and Static Casting of Selected Compositions**			
	4.1 Melt 500-lb-size heats and make centrifugal and static castings			
	4.2 Conduct mechanical properties on centrifugal and static castings poured from 500-lb-size heats			
5	**Develop an Alloy Property/Composition Predicting Software Tool for Commercial Applications**			
	5.1 Develop all correlation of properties with microstructural features and the alloy compositions			
	5.2 Develop user-friendly software that captures the property/composition correlation for H-Series stainless steels with predicting capabilities			
6	**Fabricate Prototype Components**			
	6.1 Cast tubes and other accessories needed to fabricate prototype components			
	6.2 Fabricate prototype components through machining and welding operations			
	6.3 Complete installation of the prototype components in various production applications			
7	**Meetings and Technical Reports**			
	7.1 Hold at least two technical meetings per year			
	7.2 Complete final report			

4. Results and Discussion

The results of this study are presented in three major sections:

1. study of existing commercial H-series alloys;
2. study of a new generation of ORNL alloys;
3. development of new advanced alloys.

4.1 Study of Existing Commercial H-Series Alloys

Although a wide range of H-series alloys are commercially available, this study focused primarily on HP (Fe-25Cr-35Ni) and HK (Fe-25Cr-25Ni) series alloys. As a part of this study, it was necessary to evaluate the ability of existing thermodynamic databases to predict the microstructure of the alloys and to assess the role of microstructure in determining the creep properties of the alloys. Detailed microstructural characterization was performed on the selected H-series alloys, and the ability of thermodynamic calculations to predict the observed microstructure was evaluated using qualitative and quantitative comparisons [17–18]. The results of this work showed that there was a good qualitative agreement between the microstructures of commercial alloys and thermodynamic calculations. Although some discrepancies were observed between quantitative assessments of microstructure and thermodynamic calculations, the overall agreement was reasonable considering the approximations used in performing these comparisons. In the following pages, we present the details of the analyses.

4.1.1 Selection of Existing Commercial H-Series Alloys

Figure 4.1 shows the creep rupture life of selected commercially available H-Series alloys at 1800°F (982°C) and stresses of 3 ksi and 4 ksi as measured in this project. Note that the creep rupture life varies over a wide range (from less than 100 to 1800 h) depending on the composition of the alloys. To understand the role of microstructure in the creep properties of these alloys, it was decided that two alloys with widely different creep properties would be selected and the microstructure of these alloys would be examined. Alloy 3 has the lowest creep rupture life, while alloy 2 has the highest creep rupture life among the alloys shown in Fig. 4.1. The study of these two alloys with widely different properties was expected to reveal significant differences in microstructure and outline desirable and undesirable

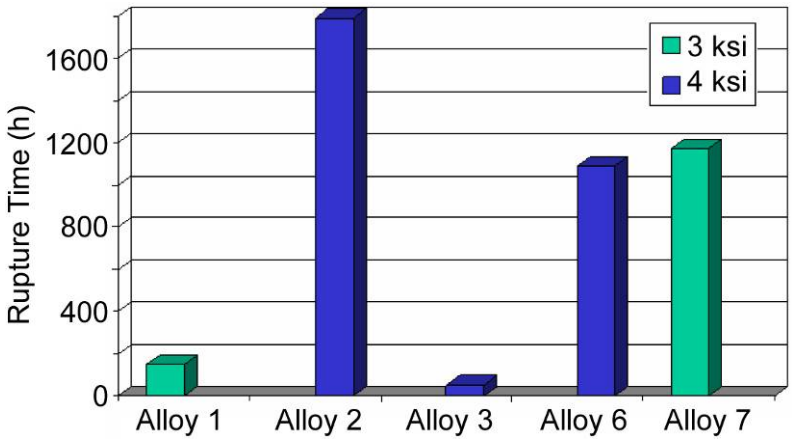

Fig. 4.1. Creep rupture life of six selected commercial H-Series alloys at 1800°F (982°C).

microstructures. Alloys 2 and 3 were thus selected for detailed study of the relationship between the microstructure and creep properties at 1800°F (982°C).

4.1.2 Thermodynamic Calculations of H-Series Alloys 2 and 3

Figure 4.2 shows results of thermodynamic calculations of the two selected alloys obtained using JMatPro. Both sections of the figure show the stability of various phases as a function of temperature in these alloys. In addition to the austenitic matrix, calculations show that three types of carbides—$M_{23}C_6$, M_7C_3, and MC—can be stable in alloy 2. In alloy 3, however, only $M_7C_3$and MC-type carbides are predicted to be stable, with no $M_{23}C_6$-type carbides being present in the alloy at any temperature. Detailed microstructural characterization was necessary to verify the results of these thermodynamic calculations. The results are presented below.

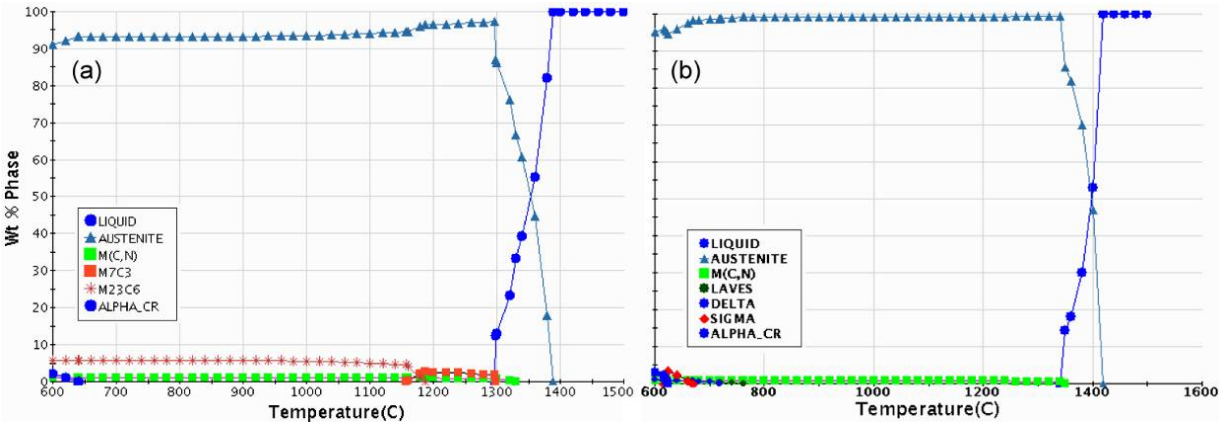

Fig. 4.2. Thermodynamic calculations using JMatPro predict differences in carbide precipitation between alloy 2 (a) and alloy 3 (b).

Figure 4.3 shows optical microscopy images of specimens from alloys 2 and 3. The specimens were obtained from creep specimens exposed to 1800°F (982°C) but away from the region of failure. The higher density of precipitates in the specimens from alloy 2 than the alloy 3 specimens is the first major difference observed in the microstructure of the two alloys with widely different properties.

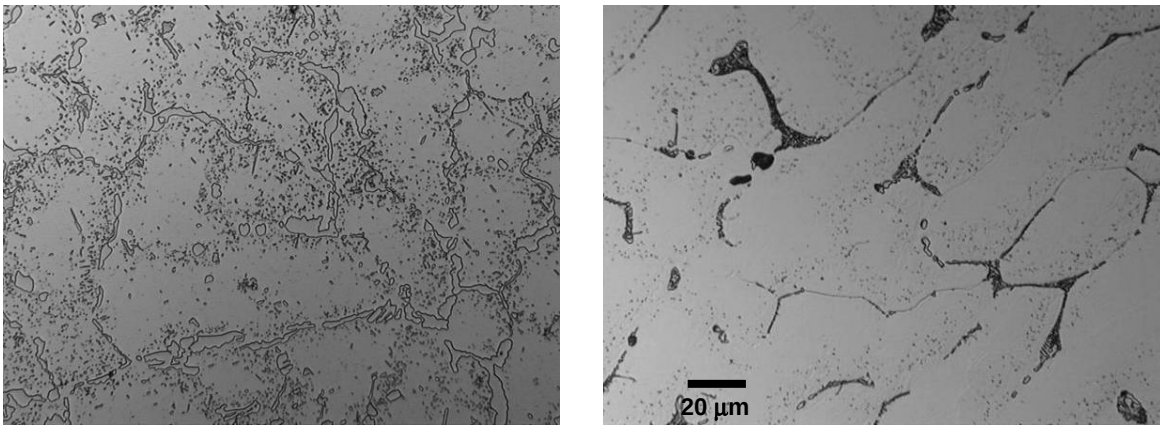

(a) Alloy 2 **(b) Alloy 3**

Fig. 4.3. Optical microscopy images of alloys 2 and 3 after creep testing at 1800°F (982°C) showing more precipitation in alloy 2 than in alloy 3.

Figure 4.4 shows an optical microscopy image and a back-scattered scanning electron microscope (SEM) image from alloy 2. At least two different types of phases with different contrasts can be observed in these samples in addition to the austenitic matrix. Detailed energy-dispersive X-ray analysis (Fig. 4.5) shows that the darker phase is $M_{23}C_6$-type carbide, while the brighter phase is the MC-type carbide that is rich in niobium.

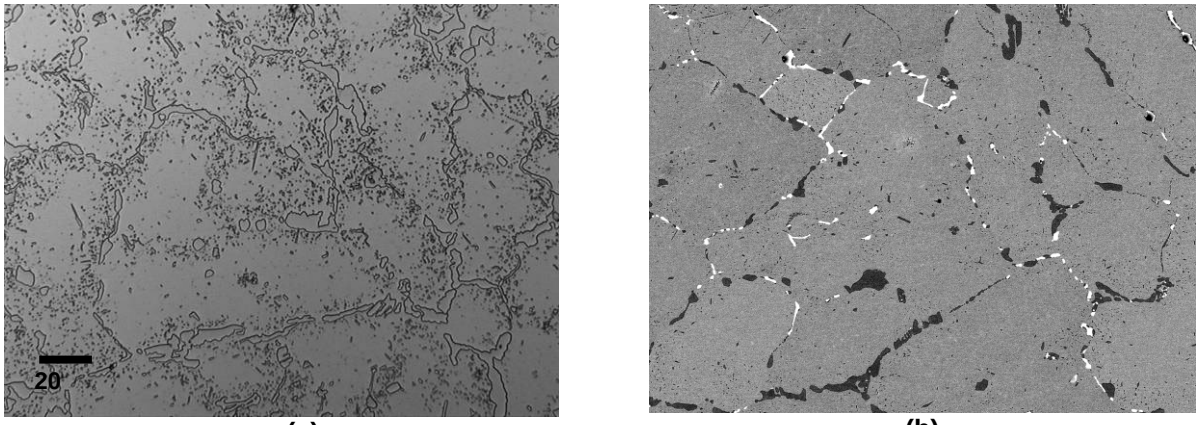

Fig. 4.4. (a) Optical and (b) back-scattered scanning electron microscope image of alloy 2 showing the presence of at least two types of phases in this alloy.

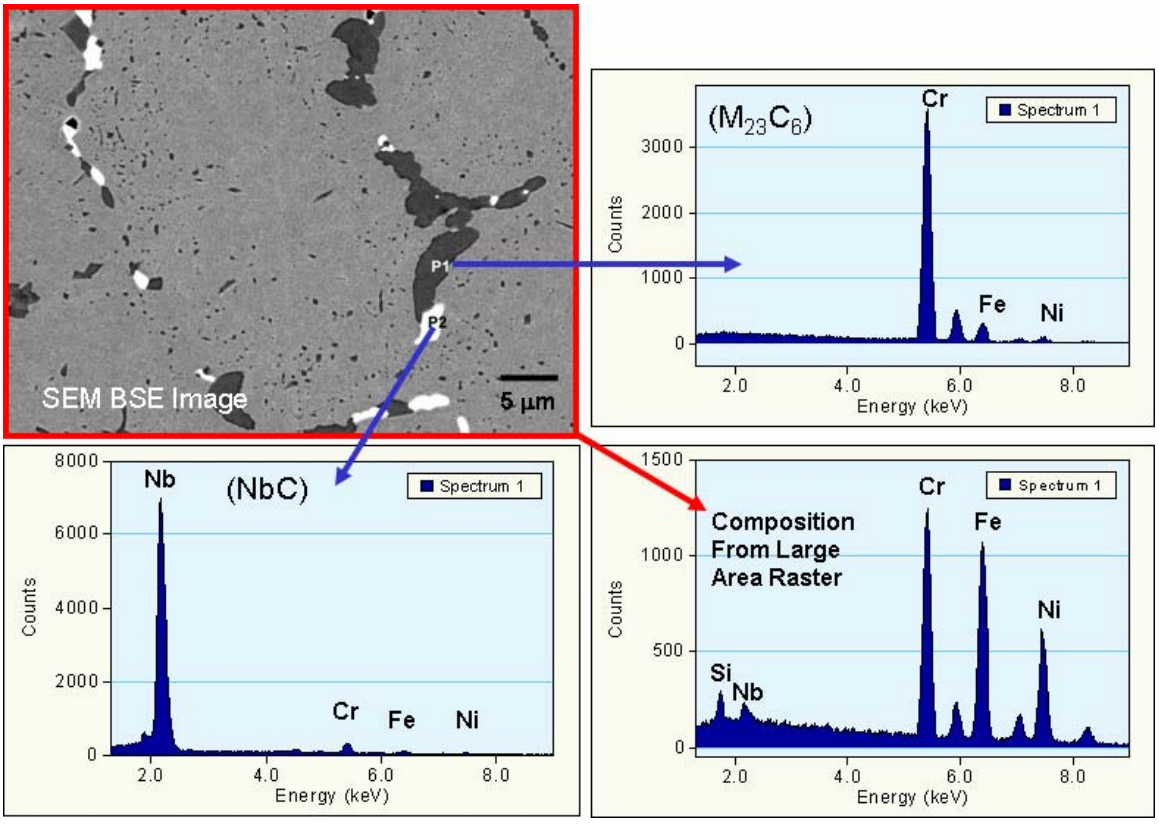

Fig. 4.5. Energy-dispersive X-ray analyses via SEM reveal the phases in alloy 2 as $M_{23}C_6$ and MC.

Figure 4.6 shows a comparison of back-scattered electron images obtained from specimens of alloys 2 and 3. The microstructure of alloy 3 clearly shows that it lacks the darker phase, $M_{23}C_6$, which is present in alloy 2. As can be seen from the figure, only NbC is prominent in alloy 3.

Most of the results on microstructure presented above are on a coarse scale. It is well understood that the fine-scale microstructure has a significant effect on creep properties. Figures 4.7 and 4.8 show scanning and transmission microscopy images of alloy 2 which show the presence of both $M_{23}C_6$ and MC near the grain boundaries and within the grain. By contrast, transmission electron microscopy reveals some precipitation of MC only near the grain boundaries in alloy 3 with very little precipitation within the grains (Figs. 4.9 and 4.10). Two major differences have been observed in the microstructure of alloys 2 and 3:

1. There was significantly more precipitation in alloy 2, which had better creep properties, than in alloy 3.
2. $M_{23}C_6$ precipitates were absent in alloy 3, the alloy with inferior creep properties. The lack of $M_{23}C_6$ precipitates is also consistent with the predictions of thermodynamic calculations.

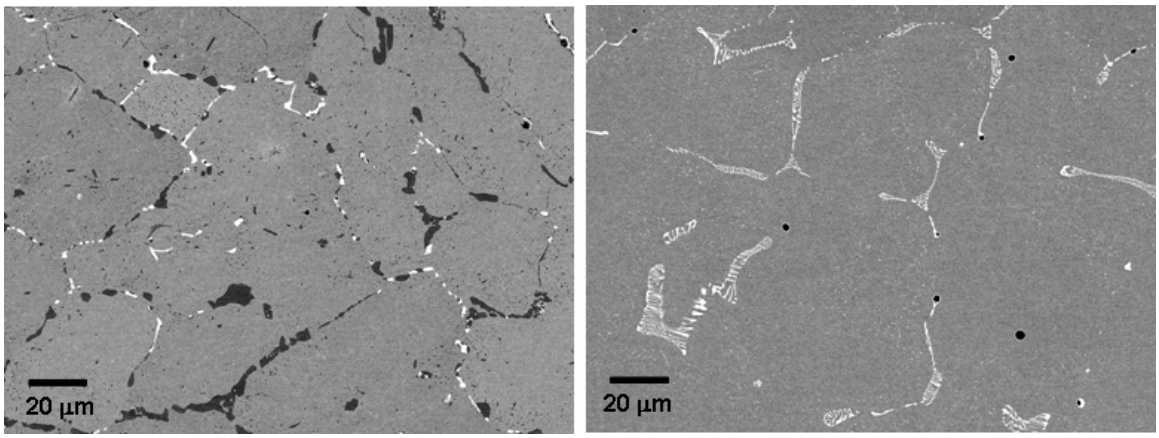

(a) Alloy 2 **(b) Alloy 3**

Fig. 4.6. Back-scattered electron imaging of alloys 2 and 3 reveals the presence of only interdendritic and matrix NbC (bright regions) in alloy 3.

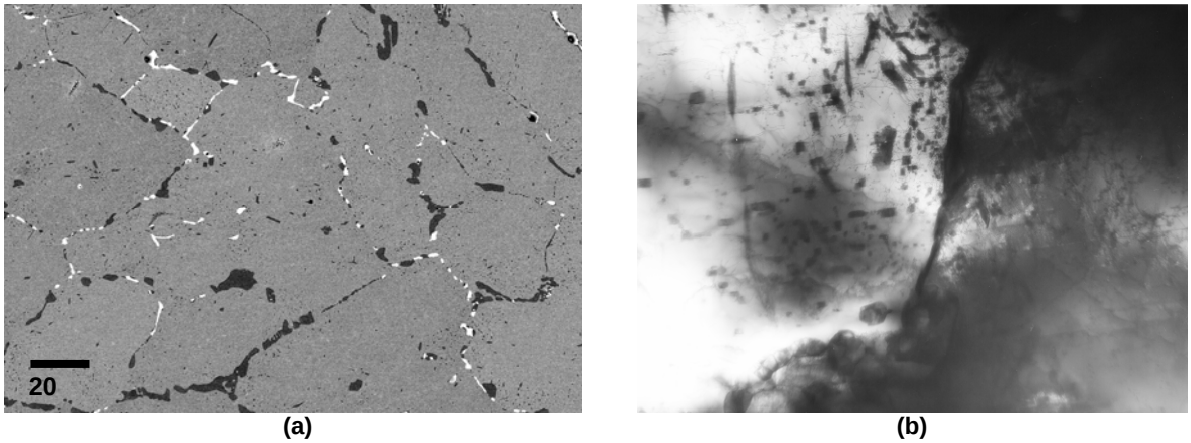

(a) **(b)**

Fig. 4.7. (a) Scanning and (b) transmission electron microscope image of alloy 2 revealing precipitation of both MC and $M_{23}C_6$ near grain boundaries during creep testing at 1800°F (982°C).

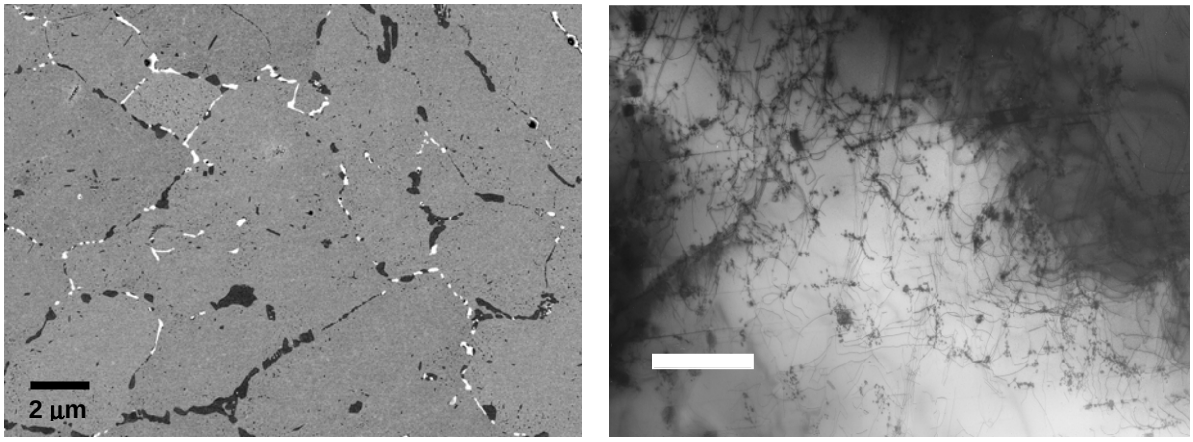

Fig. 4.8. Scanning (left) and transmission electron (right) microscopy images of alloy 2 revealing precipitation of uniform MC and $M_{23}C_6$ within the grain during creep testing at 1800°F (982°C).

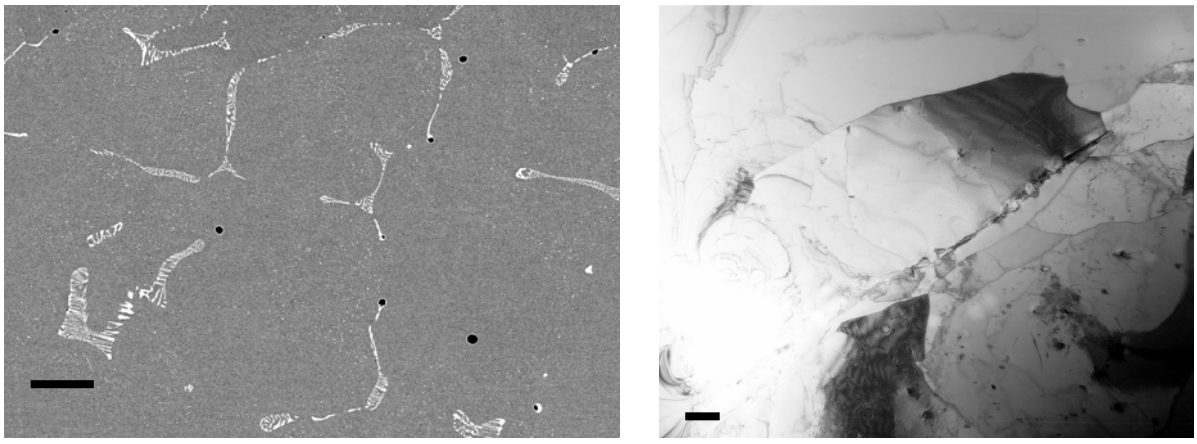

Fig. 4.9. Scanning (left) and transmission electron (right) microscopy images of alloy 3 revealing precipitation of only MC near the grain boundaries during creep testing at 1800°F (982°C).

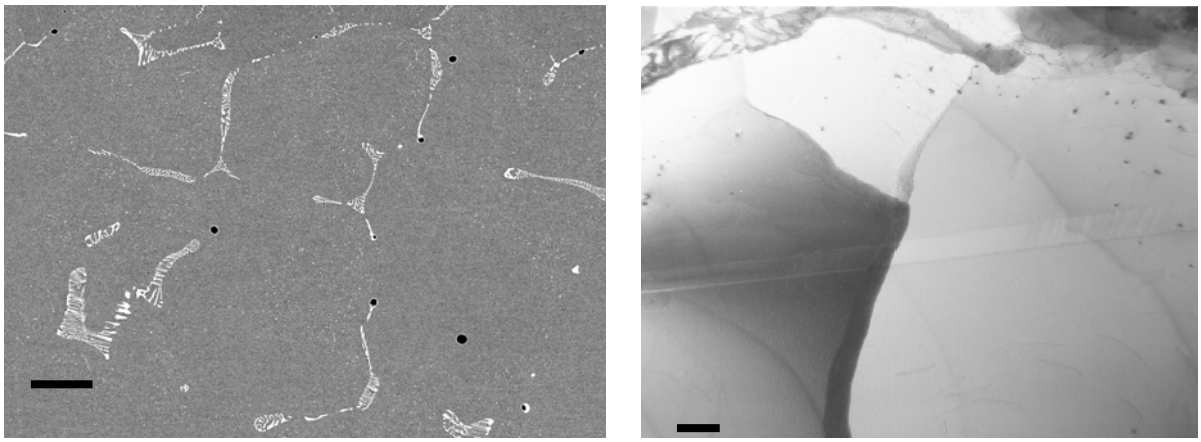

Fig. 4.10. Scanning (left) and transmission electron (right) microscopy images of alloy 3 revealing little fine precipitation within the grains during creep testing at 1800°F (982°C).

4.1.3 Validation of Thermodynamic Calculations Using Quantitative Microscopy

As pointed out above, comparison of the prediction obtained from thermodynamic calculations with results from microstructural characterization clearly shows good qualitative agreement. To further evaluate the accuracy of calculations, it was decided to test whether quantitative agreement would be obtained between the observed and predicted volume fraction of phases. To enable this comparison, volume fractions of phases in alloys 2 and 3 were obtained by measuring the area fraction of phases in a back-scattered electron image. This was achieved by using the differences in contrast between the darker $M_{23}C_6$ phase and the brighter MC phase. Regions of the two phases were identified using contrast values appropriate to the phase of interest, and the corresponding area fractions were calculated in the binary image. Figure 4.11 shows examples of images where contrast thresholding has been used to delineate the matrix and the two carbide phases. The darker $M_{23}C_6$ phase has been identified and colored blue, while the brighter MC phase is colored yellow.

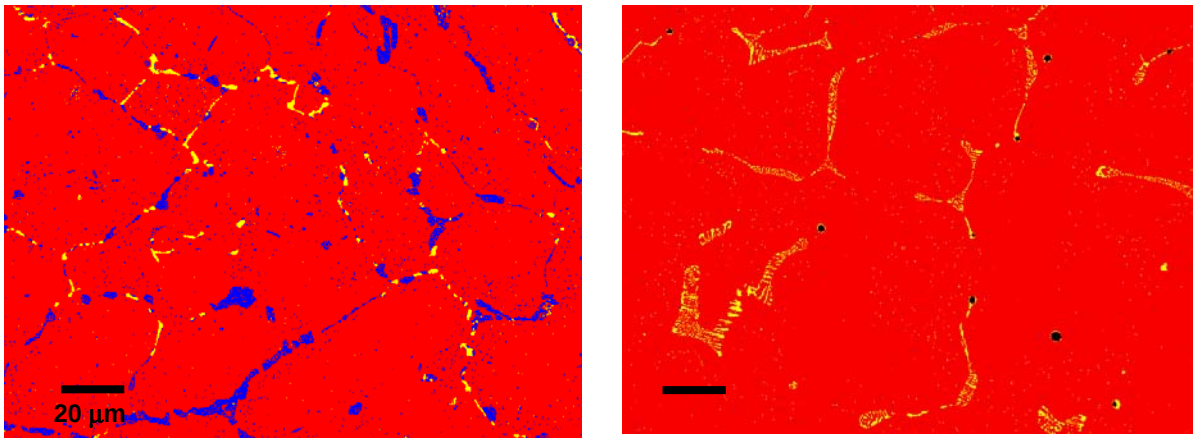

Fig. 4.11. Threshold image showing areas of austenitic matrix (red), $M_{23}C_6$(blue) and MC (yellow) in (a) alloy 2 and (b) alloy 3.

Table 4.1 shows a quantitative comparison between the weight fractions of phases predicted by equilibrium thermodynamic calculations and the measured volume fractions of phases obtained using the methodology explained above. For the purposes of the weight fraction calculations, it is assumed that the densities of the phases are comparable. Note that the comparison between the experimental measurements and equilibrium volume fractions is valid only if equilibrium is reached at the temperature of interest. Table 4.2 shows a similar comparison between the predictions of Scheil calculations [14–16] and the measured volume fractions. Scheil calculations assume local equilibrium during solidification and will tend to reflect the as-solidified microstructure rather than the equilibrium microstructure that would be obtained after prolonged exposure at a high temperature.

Comparison shows that although some discrepancies exist, there is reasonable agreement between calculations and measurement. Particularly relevant is that alloy 3 is predicted to be void of $M_{23}C_6$, which has been observed to be experimentally valid. The measured $M_{23}C_6$ contents of alloy 2 are between the values predicted by Scheil and the equilibrium calculations. This can be explained on the basis that equilibrium may not have been completely achieved during creep testing at 1800°F (982°C).

Table 4.1. Weight fraction of phases predicted using equilibrium thermodynamic calculations and measured volume fraction of phases at 1800°F (982°C) for commercial alloys 2 and 3

Alloy designation	Austenite (γ)		Chromium-rich carbides $M_{23}C_6/M_7C_3$		Niobium-rich carbides MC		Other
	Predicted wt %	Average measured vol %	Predicted wt %	Average measured vol %	Predicted wt %	Average measured vol %	Predicted wt %
Alloy 2	93.5	95	5.5	4.0	1.0	1.0	0
Alloy 3	99.1	98.3	0	0	0.9	1.7	0

Table 4.2. Weight fraction of phases predicted using Scheil calculations and measured volume fraction of phases for commercial alloys 2 and 3

Alloy designation	Austenite (γ)		Chromium-rich carbides $M_{23}C_6/M_7C_3$		Niobium-rich carbides MC		Other
	Predicted wt %	Average measured vol %	Predicted wt %	Average measured vol %	Predicted wt %	Average measured vol %	Predicted wt %
Alloy 2	95.9	95.0	3.2	4.0	0.9	1.0	0
Alloy 3	98.8	98.3	0	0	0.6	1.7	0.6

4.1.4 Relationship between Microstructure and Creep Properties in Commercial H-Series Alloys

The results presented above indicate significant differences in the amount of carbide phases present in alloys 2 and 3. Since alloy 2 has a significantly better creep rupture life at 1800°F (982°C), it can be concluded that carbide phases have a positive effect on the creep rupture life of H-series alloys. Furthermore, alloy 2 has two major types of strengthening carbides, while alloy 3 lacks precipitation of $M_{23}C_6$. Thus, the presence of the two carbide phases appears to be more desirable than the presence of only one type of carbide.

To summarize, based on the results of detailed thermodynamic calculations and the microstructural characterization of selected commercial H-series alloys, one may reach the following conclusions:

1. Thermodynamic calculations are reliable for the qualitative prediction of microstructure.
2. Quantitative comparisons between thermodynamic calculations and microstructure show reasonable agreement, with occasional discrepancies.
3. Alloys that contain both $M_{23}C_6$ and MC in their microstructures have better creep properties.

Based on the observations of the relationship between carbides and creep properties, a first generation of new alloys was prepared at ORNL. The newly designed alloys were melted into 25- to 50-lb heats and cast into slabs. Test bars from experimental heats were creep-tested at 2200°F (1204°C), with some tests done at lower temperatures; one test was done at 2300°F (1260°C). Further work was carried out to study the relationship between the composition, microstructure, and creep properties of some of these alloys, as discussed in the following sections.

4.2 Study of Trial ORNL HP-Alloys with Different Niobium Contents

Preliminary studies of the effect of alloying elements in existing alloys showed that the addition of niobium improved the creep properties of H-series alloys. Two alloys with different niobium contents were cast in small batches at ORNL to study the effect of niobium additions on HP-type alloys. The compositions of these alloys are shown in Table 4.3.

Table 4.3. Composition of trial HP alloys with high niobium contents

Alloy designation	C	Cr	Ni	Mn	Si	Nb	W	Fe
HP-1	0.4	22.7	34.6	0.8	1.5	1.0	0.1	Bal.
HP-2	0.4	23.0	35.2	0.8	1.5	2.1	0.1	Bal.

Detailed thermodynamic calculations along with microstructural characterization were carried out to study the microstructure in these alloys and to evaluate the effect of the microstructures on the creep properties of these two alloys.

Thermodynamic calculations. Thermodynamic calculations were performed to understand the stability of various phases at equilibrium in alloys HP-1 and HP-2 as a function of temperature. The results are shown in Figs. 4.12 and 4.13. In addition to austenite, carbides such as $M_{23}C_6$, MC, and M_7C_3 were predicted to be important over the temperature range of interest, which is consistent with observations from previous experimental studies. Relative to HP-2, $M_{23}C_6$ is predicted to be present in larger fractions in HP-1 along with a smaller amount of MC-type carbides in the temperature range 1472 to 2012°F (800 to 1100°C). By contrast, $M_{23}C_6$ and MC-type carbides are predicted to be present in comparable weight fractions in alloy HP-2 over the same temperature range, indicating a much larger MC-content in alloy HP-2. Thus, it is expected that MC-type carbides will play a significantly larger role in affecting the mechanical properties of alloy HP-2 than those of alloy HP-1. Furthermore, the total carbide content in HP-2 is smaller than that in HP-1. The effect of carbide contents on creep properties is discussed below.

Microstructural characterization. Microstructural characterization was carried out to verify the predictions of the thermodynamic calculations. Figure 4.14 shows a typical backscattered scanning electron micrograph obtained from the as-cast specimens of HP-1 and HP-2. In Fig. 4.14(a), large carbides can be seen both along the seams between the colonies of dendrites and in the interdendritic regions. Precipitates appearing brighter than the matrix have been identified, using energy-dispersive X-ray spectrometry, as niobium-rich MC-type carbides/carbonitrides, while those appearing dark have been identified as chromium-rich carbides. Figure 4.14(b) shows the corresponding back-scattered electron image from as-cast HP-2 alloy. In contrast to the micrograph for the HP-1 alloy, Fig. 4.14(b) shows an increase in the amount of the bright MC-type carbides. A similar conclusion can be reached by comparing the X-ray diffraction patterns from these two alloys shown in Fig. 4.15.

Quantitative microscopy. To enable a quantitative comparison between the predictions and the observed as-cast microstructure, Scheil calculations were performed for both alloy compositions. Table 4.4 summarizes the Scheil predictions for phases present in the solidified alloys and the average values measured from image analysis of backscattered electron images of the as-cast specimens. Again, weight fractions have been assumed to be equal to volume fractions. The predictions for the HP-1 alloy are in reasonable agreement with measured values. However, for the HP-2 alloy, although the effect of increasing the niobium content is qualitatively consistent with an increase in the fraction of MC carbides, the measured fraction of MC-type carbides is much larger than the predicted values.

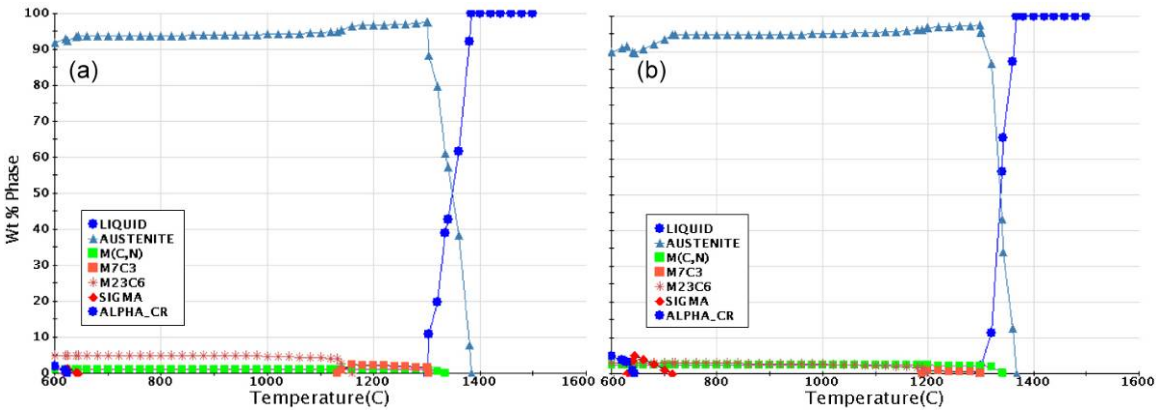

Fig. 4.12. Thermodynamic calculations as a predictor of differences in carbide precipitation between (a) HP-1 and (b) HP-2.

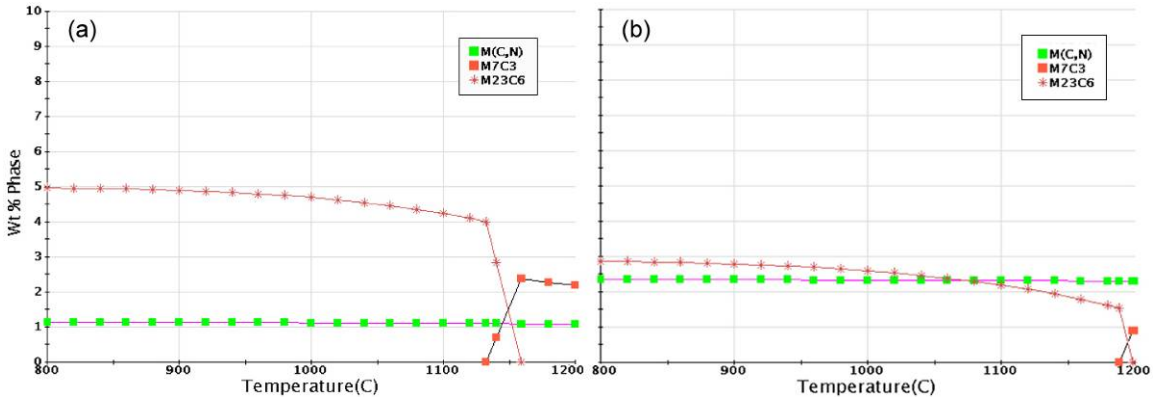

Fig. 4.13. Expanded view of Fig. 4.12 showing carbide phases and phase fractions predicted to be present over the temperature range 1472 to 2192°F (800 to 1200°C) in (a) HP-1 and (b) HP-2. Note the decrease in the amount of $M_{23}C_6$ and increase in amount of MC in HP-2 when compared to HP-1.

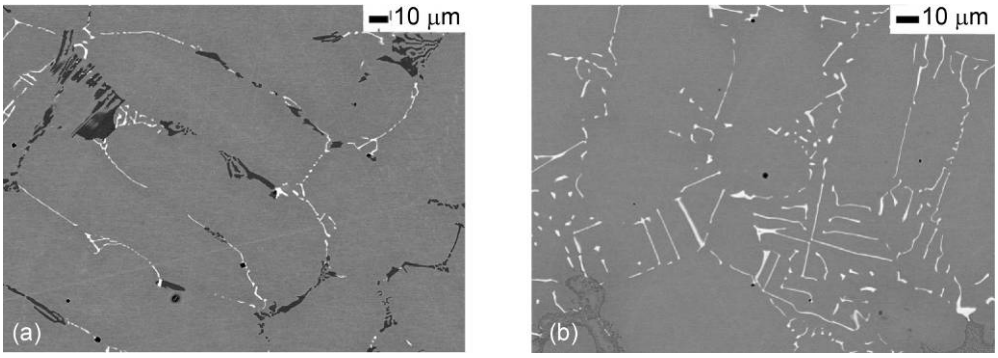

Fig. 4.14. Backscattered scanning electron micrographs of (a) as-cast HP-1 and (b) as-cast HP-2 showing the presence of both niobium-rich carbides (bright) and chromium-rich carbides (dark) in HP-1 and of predominantly niobium-rich carbides in HP-2.

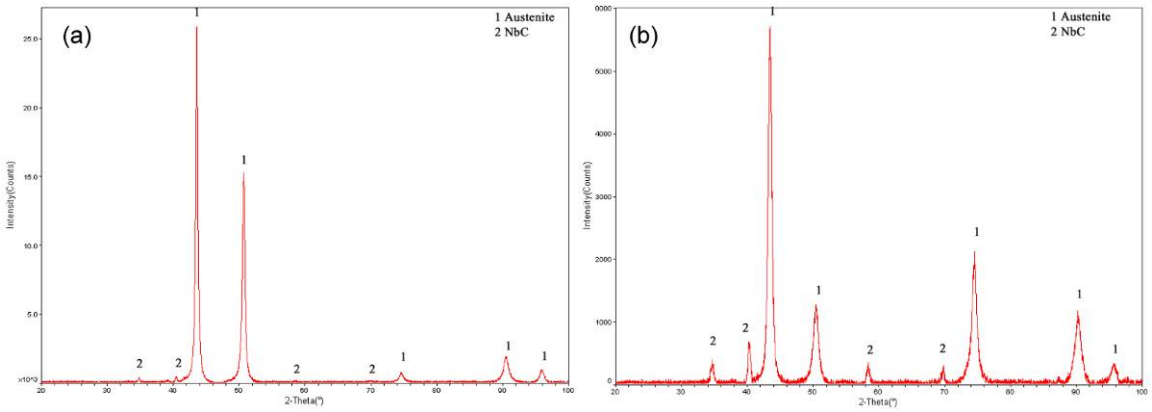

Fig. 4.15. X-ray diffraction patterns from (a) as-cast HP-1 and (b) as-cast HP-2 showing the presence of austenite in both samples and an increase in the intensity of NbC peaks in (b).

Table 4.4. Phase contents predicted using Scheil calculations and actual measured values in as-cast microstructure for trial alloys HP-1 and HP-2

Alloy designation	Austenite (γ)		Chromium-rich carbides $M_{23}C_6/M_7C_3$		Niobium-rich carbides MC		Other
	Predicted wt %	Average measured vol %	Predicted wt %	Average measured vol %	Predicted wt %	Average measured vol %	Predicted wt %
HP-1	96.6	95.1	2.5	3.7	1.0	1.2	0
HP-2	96.0	95.0	1.7	0.7	2.1	4.3	0.3

A comparison of the microstructure observed in the as-cast state with the Scheil calculations shows that the thermodynamic calculations are qualitatively consistent with the observed microstructure of alloys HP-1 and HP-2. For example, the amounts of chromium-rich carbides are predicted to be more than the amount of MC-carbides in HP-1; this prediction is verified by the evaluation of the microstructure. The prediction that the amount of MC carbides would be larger than the amount $M_{23}C_6$ carbides in HP-2 is also borne out by the observed microstructure; however, the observed microstructure shows a much larger amount of MC carbides than what is predicted, and hence, there is a discrepancy between the calculations and the observed microstructure. Again, it can be concluded that thermodynamic calculations are qualitatively correct but may be quantitatively different from the observed microstructure.

Creep testing. Figure 4.16 shows the results of creep testing of HP-1 and HP-2 at stresses ranging from 7 to 27.6 MPa (1 to 4 ksi) at temperatures of 1800°F (982°C) and 2000°F (1093°C). Results clearly show that alloy HP-1 has better creep resistance than HP-2, particularly at 1093°C and 6.89 MPa, where HP-1 has about 1.5 times longer rupture life than HP-2. This is significant because HP-1 has only half the niobium content of HP-2. Microstructural analysis provides additional insight as to why less niobium results in better creep behavior.

Microstructural characterization. Microstructural changes occur when the as-cast structure is exposed to high temperatures during creep testing. It was important to evaluate these microstructural changes to relate them to the improved properties of HP-1. To understand this evolution and evaluate its effect, a quantitative study of the phase fractions was carried out on specimens that were tested at 1800°F (982°C).

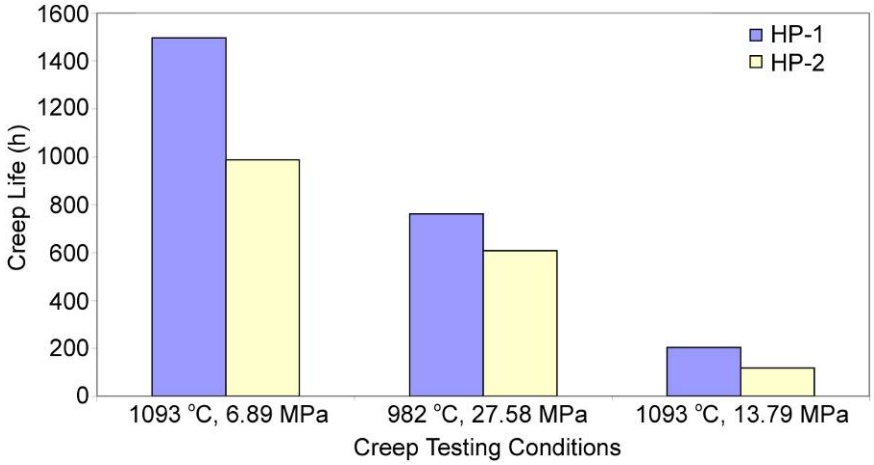

Fig. 4.16. Results of creep testing for HP-1 and HP-2 alloys at different temperatures and stress levels. As can be seen, HP-1 has better creep properties than HP-2.

Figure 4.17(a) shows a backscattered electron micrograph from an HP-1 sample that was exposed to 1800°F for 762 h (time to failure). Some breakdown of the as-cast microstructure can be observed, along with an increase in the globular nature of the phases. Figure 4.17(b) shows the corresponding micrograph obtained from an HP-2 sample, but after a shorter time to failure (608 h of exposure). Comparison with the as-cast microstructure again shows some spheroidization of the phases. Qualitatively, however, the microstructure was similar to that observed in the as-cast condition. Thus, it was necessary to evaluate the effect of the high-temperature exposure on the amounts of $M_{23}C_6$ and MC in the two alloys; the results of this evaluation are discussed next.

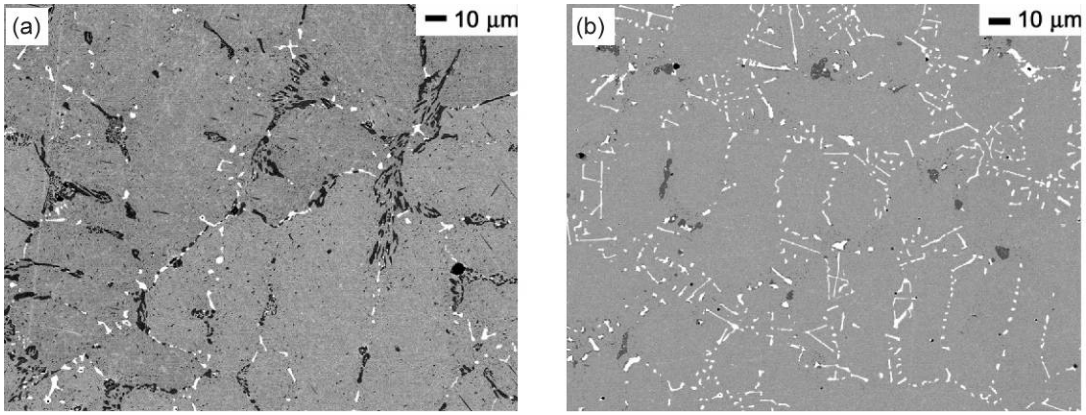

Fig. 4.17. Backscattered scanning electron micrograph obtained from (a) HP-1 and (b) HP-2 after creep failure at 1800°F (982°C).

Quantitative microscopy. Table 4.5 shows a comparison between the observed phase fractions in HP-1 and HP-2 with that predicted by equilibrium thermodynamic calculations. Although region-to-region variations were prevalent, there was good quantitative agreement between the predictions and the average measurements for HP-1. In the case of HP-2, although there was good qualitative agreement between the predictions and the observed microstructure, quantitative measurements show a larger amount of MC-type carbides and a smaller amount of $M_{23}C_6$ than predicted by thermodynamic calculations. It is likely that the carbon is tied up in the stable MC-phase due to its precipitation under

the nonequilibrium conditions prevailing during solidification, thus limiting further precipitation of $M_{23}C_6$ during exposure to high temperatures.

Table 4.6 provides a comparison of the volume fractions of the various carbides observed after creep testing with those observed in the as-cast structure. From the data provided in this table, it can be inferred that the volume fraction of $M_{23}C_6$ increased in both alloys after exposure to 1800°F (982°C), with the increase in the HP-1 alloy being much larger than that observed in HP-2. Correlation of the creep properties with the relative phase fractions of $M_{23}C_6$ and MC clearly shows that $M_{23}C_6$ plays an important role in improving the creep properties of these alloys. This observation is consistent with a previous study [17] that showed that some $M_{23}C_6$ is essential for improving the creep properties of H-series alloys.

The use of thermodynamic calculations offers the possibility of obtaining quantitative relationships between precipitation and coarsening of various phases, and the creep properties. As can be seen from Table 4.6, the alloy that had significant $M_{23}C_6$ precipitation at the creep testing temperature (alloy HP-1) also had improved creep properties. The study of creep properties and microstructural evolution occurring in these alloys at 2000°F (1093°C) leads to similar conclusions. Figure 4.18 shows the calculated amounts of $M_{23}C_6$ and MC carbides present in the alloys at equilibrium and after solidification, as well as the extent of precipitation occurring during exposure to the temperature of creep tests. Figure 4.19 shows equivalent data for MC-type carbides. As can be observed in these figures, the creep properties of the alloys correlate better with the precipitation of $M_{23}C_6$ than with the precipitation of MC, illustrating that precipitation of $M_{23}C_6$ is essential for improved creep resistance.

Given these findings, the following conclusions can be drawn:

- Larger amounts of carbide typically result in improved creep properties.
- The presence of both $M_{23}C_6$ and MC carbides are beneficial for high-temperature creep properties.

Table 4.5. Phase contents predicted using equilibrium calculations and measured values in the microstructure as observed in fractured creep specimens for trial alloys HP-1 and HP-2

Alloy designation	Austenite (γ)		Chromium-rich carbides $M_{23}C_6$		Niobium-rich carbides M(C,N)	
	Predicted wt %	Average measured vol %	Predicted wt %	Average measured vol %	Predicted wt %	Average measured vol %
HP-1	94.1	94.2	4.7	4.8	1.1	1.1
HP-2	95.0	95.2	2.7	0.8	2.3	4.0

Table 4.6. Change in the measured volume fractions of chromium-rich and niobium-rich carbides after creep testing at 1800°F for trial alloys HP-1 and HP-2

Alloy designation	Change in measured vol %		Creep rupture life at 1800°F, 4 ksi
	Cr-rich carbides $M_{23}C_6$	Nb-rich carbides M(C,N)	
HP-1	1.01	–0.2%	762 h
HP-2	0.1	–0.3%	608 h

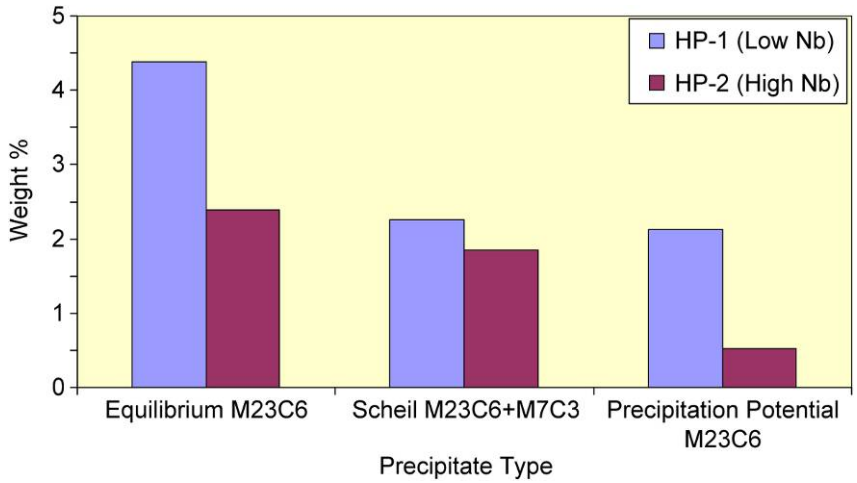

Fig. 4.18. Calculated amounts of precipitation of $M_{23}C_6$ at equilibrium during solidification and exposure to creep testing temperature of 2000°F (1093°C).

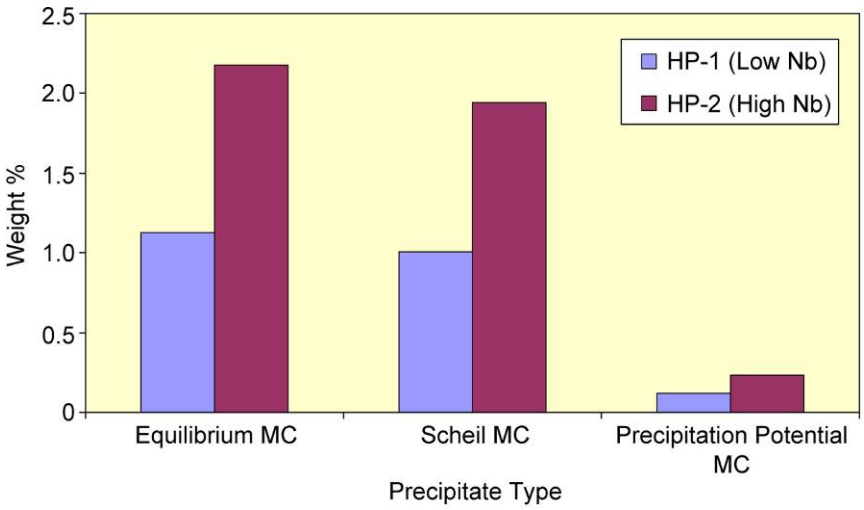

Fig. 4.19. Calculated amounts of precipitation of MC at equilibrium during solidification and exposure to creep testing temperature of 2000°F (1093°C).

These results are consistent with the observations made during the study of existing commercial H-series alloys. Hence, in the second phase of this project, baseline alloy compositions were modified using thermodynamic calculations to (1) maximize the amount of carbides, (2) maximize the amount of carbides that precipitate during creep testing, (3) generate a microstructure that would have both $M_{23}C_6$ and MC phases stable at the temperature of interest, and (4) reduce the amount of deleterious topologically closely packed phases such as sigma.

4.3 Development and Study of New Advanced Alloys

4.3.1 Methodology for Development of New Alloys

The methodology used for the development of new alloys was to consider certain reference compositions of HP and HK alloys. With these compositions as a starting point, the effect of the addition of alloying elements on the stabilities of $M_{23}C_6$ and MC were calculated using thermodynamic models. Then, various alloying elements were added in sufficient amounts to stabilize the strengthening carbide phases at the required temperature [for example, 2200°F (1204°C)] as indicated by results of the thermodynamic calculations, while minimizing the formation of deleterious topologically closely packed phases at low temperatures. The focus of studies was on high temperatures because the aim of the research was to increase the operating end use temperature of alloys. The following paragraphs describe an example of this methodology.

Figure 4.20(a) shows the thermodynamic predictions for phase equilibria in an alloy, HP-11, with poor creep performance at 2200°F (1204°C). This alloy has a creep rupture life of about 14 h at a stress of 500 psi [Fig. 4.20(b)]. As can be seen in Fig. 4.20(a), in alloy HP-11$M_{23}C_6$ carbides are predicted to be stable only up to about 2100°F (1149°C) and are replaced by M_7C_3 carbides above this temperature. The approach adopted in this work was to add alloying elements to extend the range of stability of $M_{23}C_6$ to higher temperatures.

Figures 4.21(a) and (b) show the effect of the addition of varying levels of titanium, one of the commonly used alloying elements, on the stabilities of $M_{23}C_6$ and MC in HP-11. As increasing levels of titanium are added, the $M_{23}C_6$ content in the alloy decreases, while, correspondingly, the MC content increases. The highest temperature at which $M_{23}C_6$ remains stable increases slightly with the addition of titanium. Figures 4.22(a) and (b) show the effect of the addition of varying levels of tungsten on the stabilities of the two carbides. With increasing levels of tungsten, the highest temperature of stability of $M_{23}C_6$ increases significantly along with a small increase in the weight percent of the carbide phase. Tungsten has very little effect on the MC phase, as seen in Fig. 4.22(b). Thus, if the goal were to increase the amount of MC, titanium would be desirable as an alloying element. The addition of tungsten would be important to increase the amount of $M_{23}C_6$ and to increase the alloy's temperature range of stability.

4.3.2 Thermodynamic Calculations and Creep Properties of New HP-Type Alloys

Using a computational modeling approach and the addition of alloying Mo, Nb, Ti, and W to HP-11, the ORNL team designed and prepared a new generation of HP-type alloys. Figures 4.23–4.26 show the thermodynamic stabilities of the carbide phases and the corresponding creep properties at 2200°F (1204°C) and 500 psi of stress for alloys HP-7, HP-14R1, HP-15, and HP-16. As can be seen in the top graph (a) in Figs. 4.24–4.26, the addition of alloying elements increases the highest temperature at which $M_{23}C_6$ is calculated to be stable. Figures 4.27 and 4.28 show the creep properties of the widely used commercial HP alloys Supertherm and S-22H. Figure 4.29 shows a comparison of the creep properties at 2200°F (1204°C) and 500 psi of certain ORNL alloys with commercially available alloys. It can be seen that alloys HP-7, HP-14R1, HP-15, and HP-16 show improved creep properties. Table 4.7 provides a summary of all alloys tested in this project and a summary of the testing conditions. As seen from this table, other alloys developed in this project also show creep properties better than the properties of existing alloys under a variety of other testing conditions.

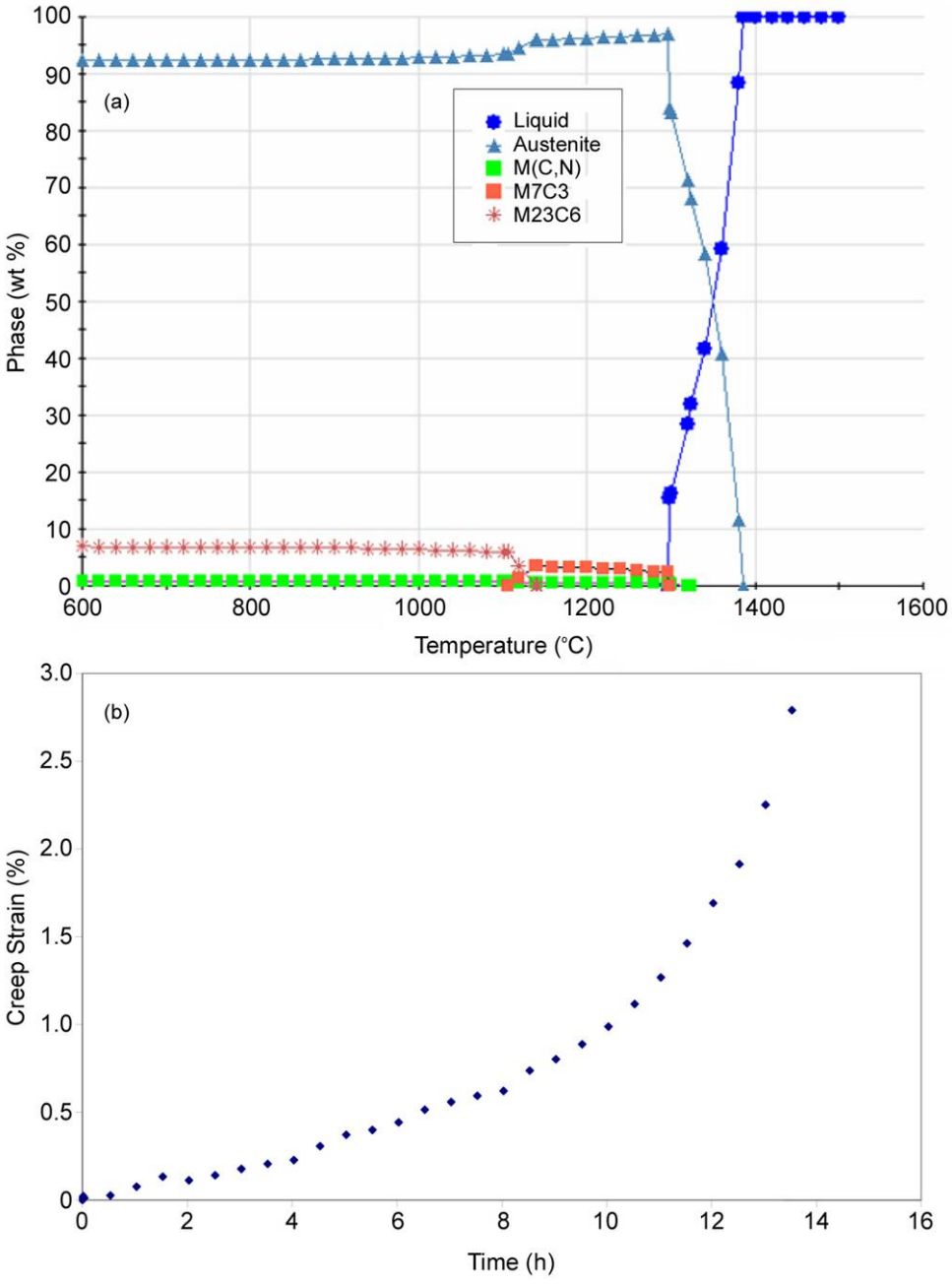

Fig. 4.20. Thermodynamic calculations and creep strain measurements for HP-11: (a) thermodynamic calculations; (b) creep strain as a function of time obtained during testing at 2200°F (1204°C) and 500 psi. Failure occurred after 14 h.

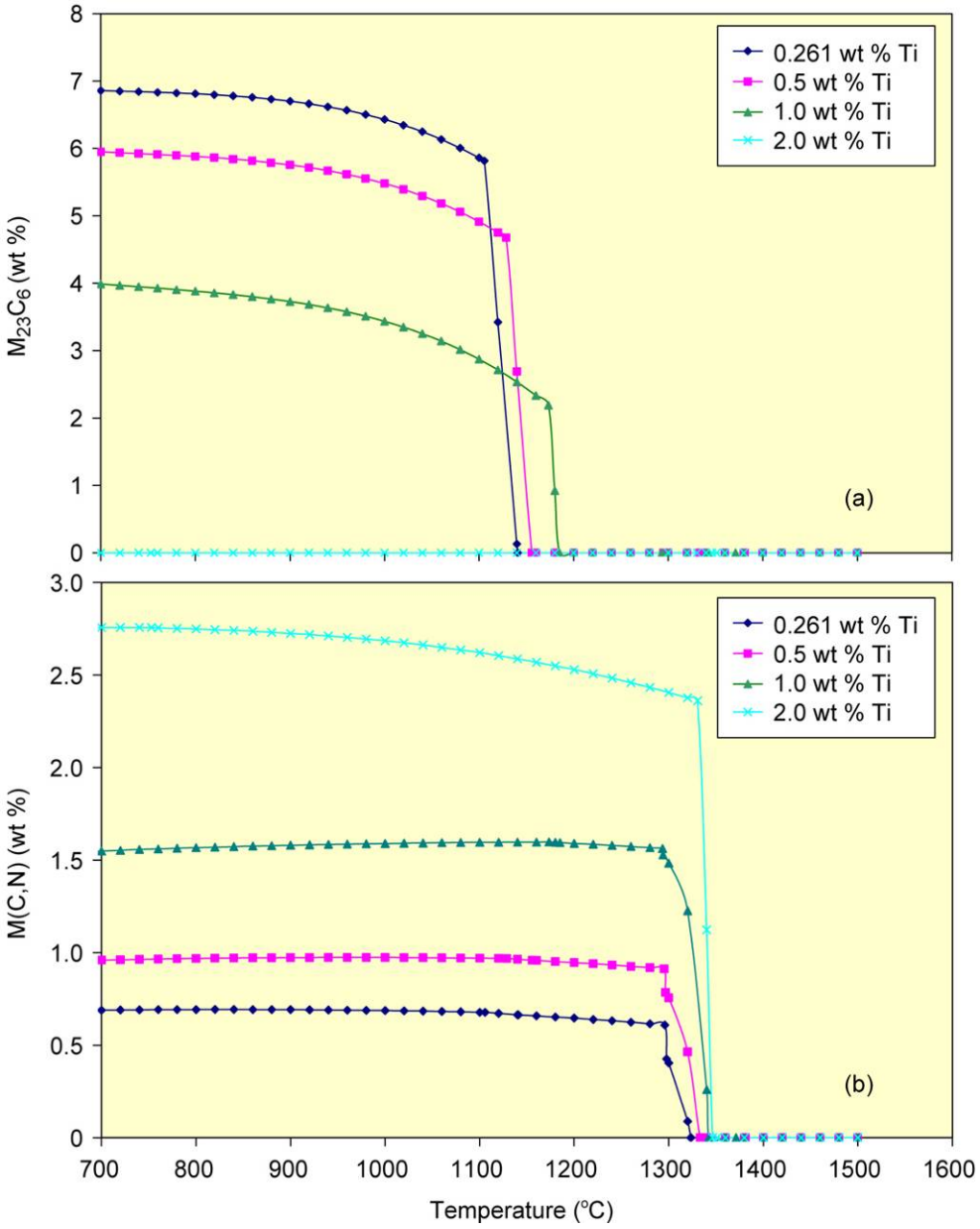

Fig. 4.21. Thermodynamic calculations showing the effect of titanium on the stabilities of $M_{23}C_6$ and MC.

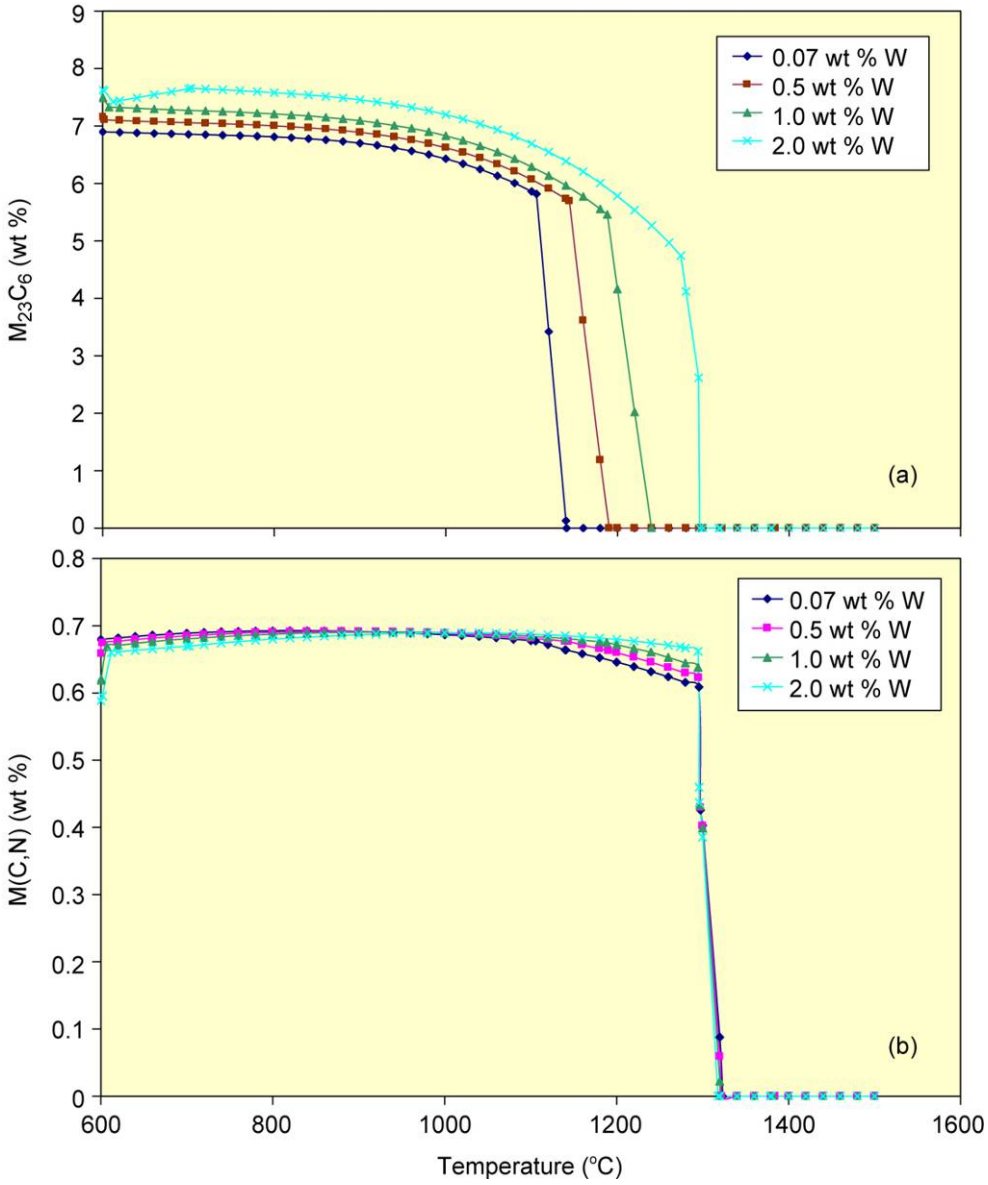

Fig. 4.22. Thermodynamic calculations showing the effect of tungsten on the stabilities of $M_{23}C_6$ and MC.

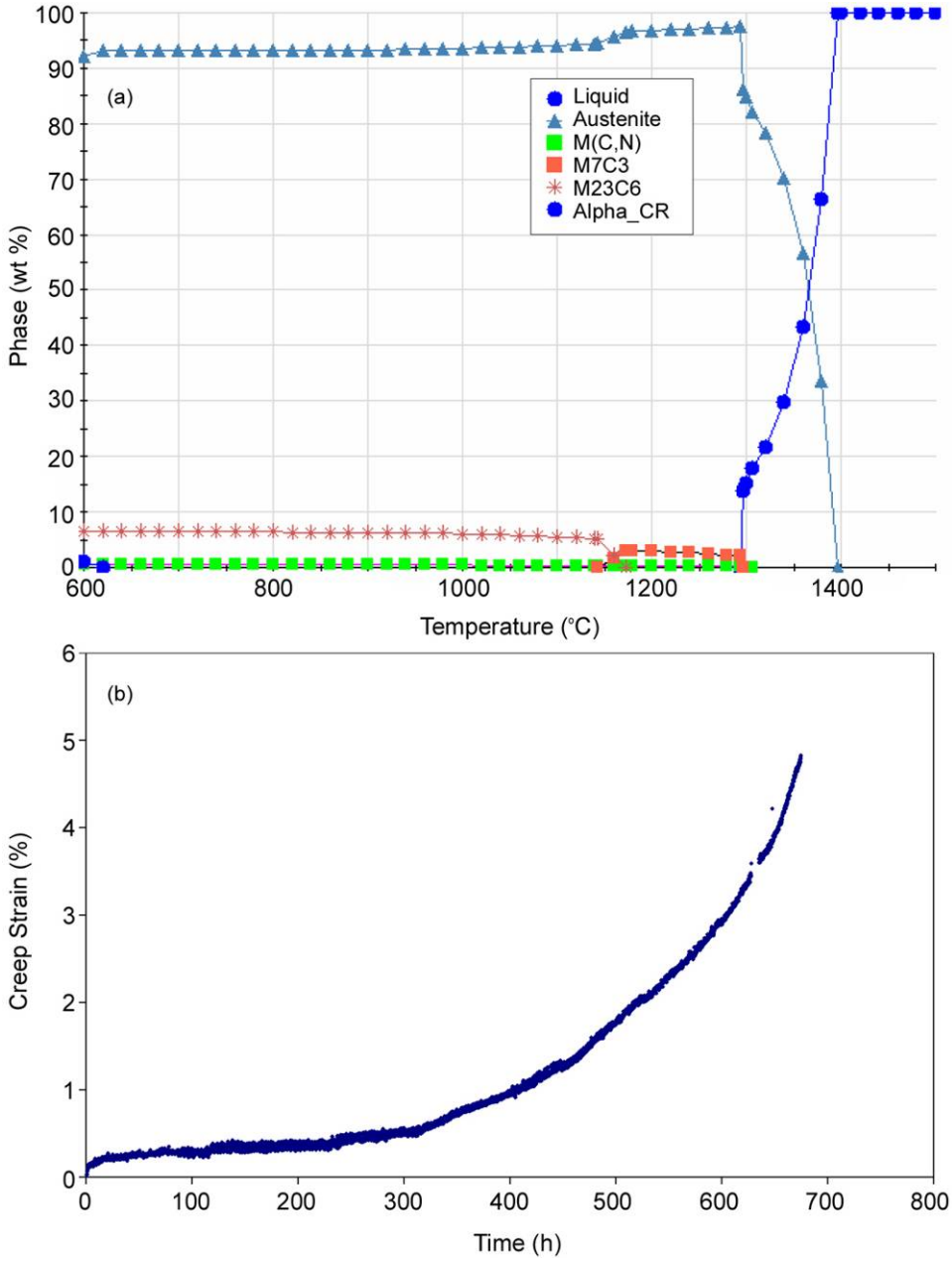

Fig. 4.23. Thermodynamic calculations and creep strain for HP-7: (a) thermodynamic calculations; (b) creep strain as a function of time obtained during testing at 2200°F (1204°C) and 500 psi. Failure occurred after 675 h.

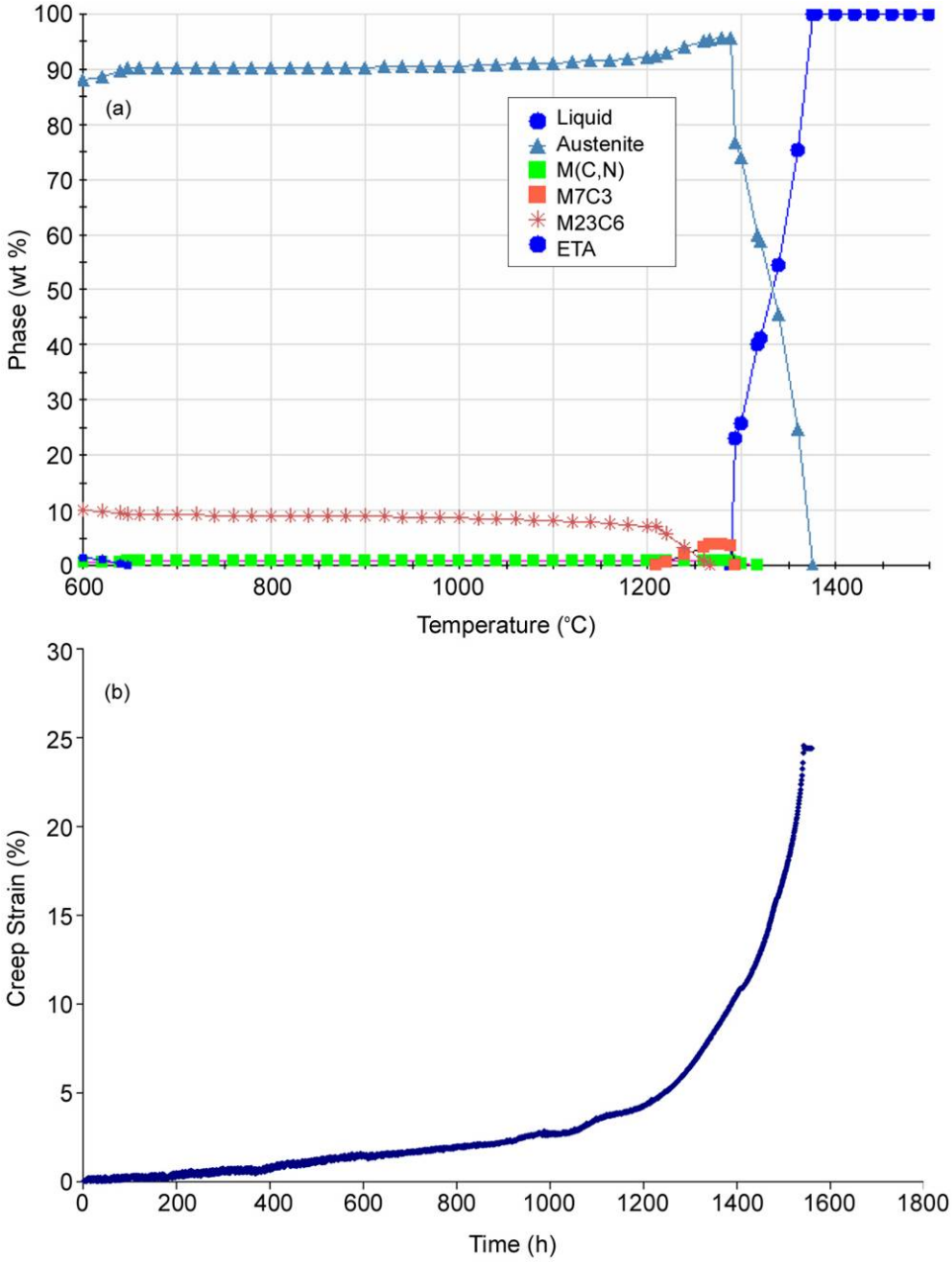

Fig. 4.24. Thermodynamic calculations and creep strain measurements for HP-14R1: (a) thermodynamic calculations; (b) creep strain as a function of time obtained during testing at 2200°F (1204°C) and 500 psi. Failure occurred after 1558 h.

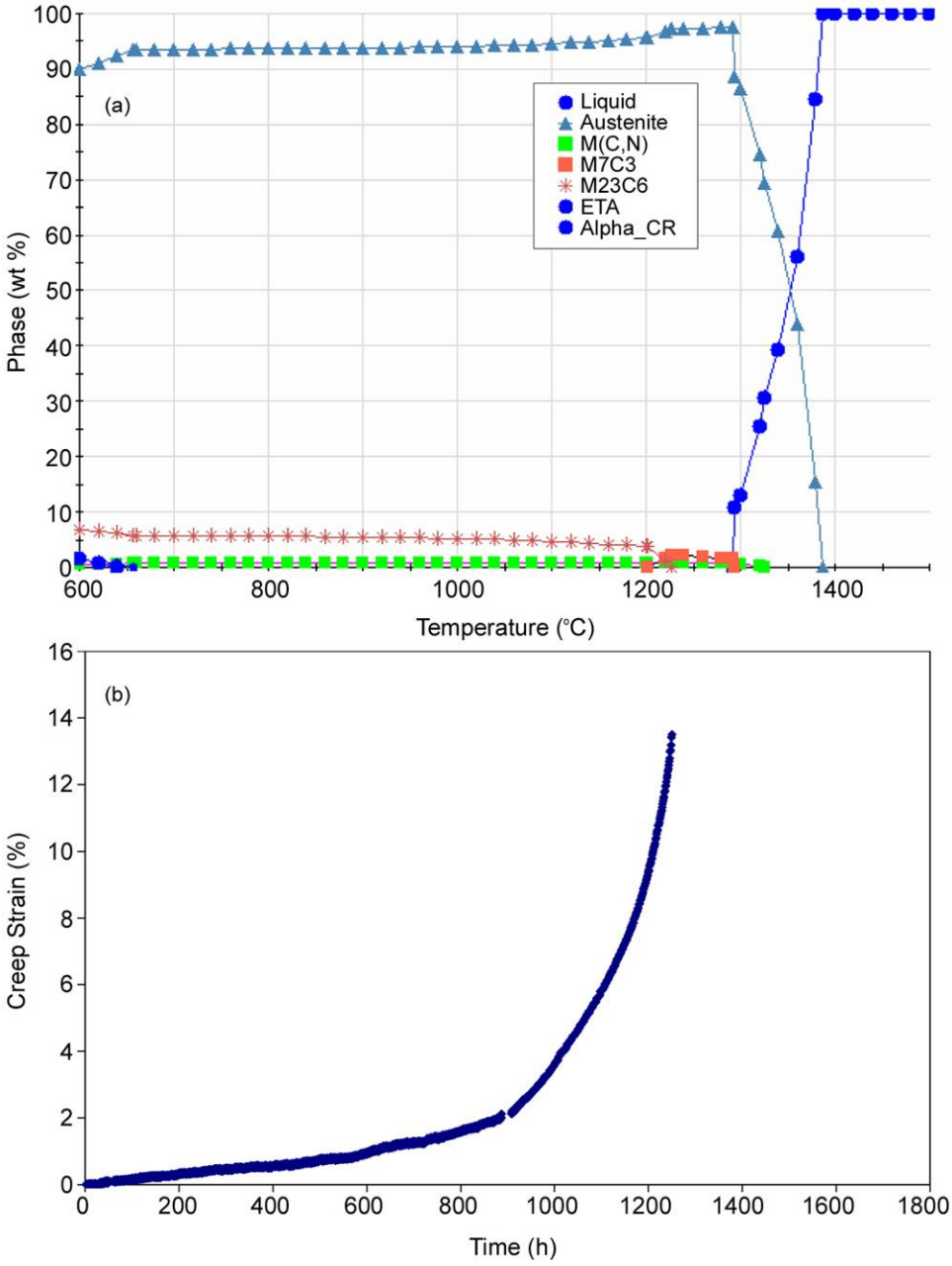

Fig. 4.25. Thermodynamic calculations and creep strain measurements for HP-15: (a) thermodynamic calculations; (b) creep strain as a function of time obtained during testing at 2200°F (1204°C) and 500 psi. Failure occurred after 1251 h.

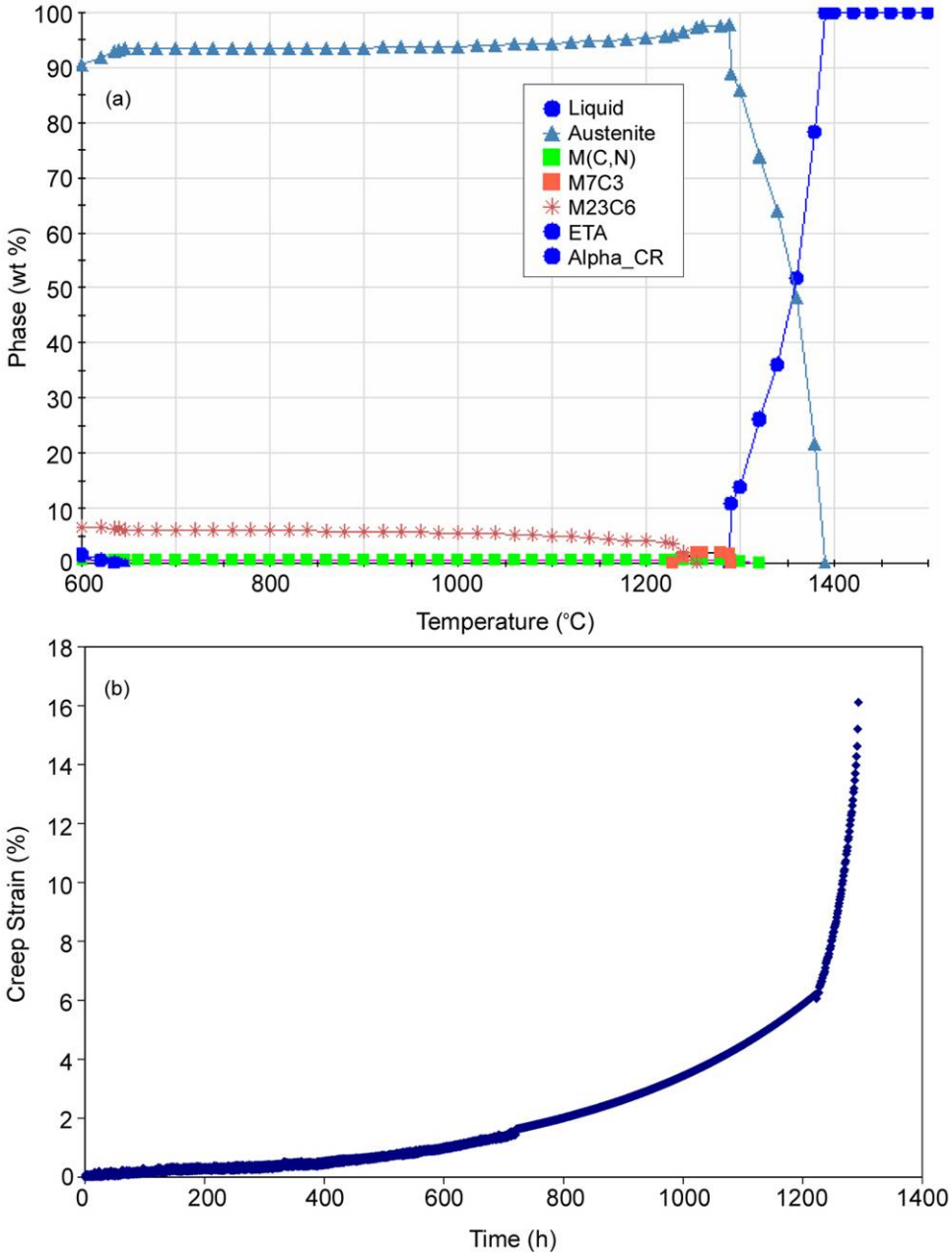

Fig. 4.26. Thermodynamic calculations and creep strain measurements for HP-16: (a) thermodynamic calculations; (b) creep strain as a function of time obtained during testing at 2200°F (1204°C) and 500 psi. Failure occurred after 1293 h.

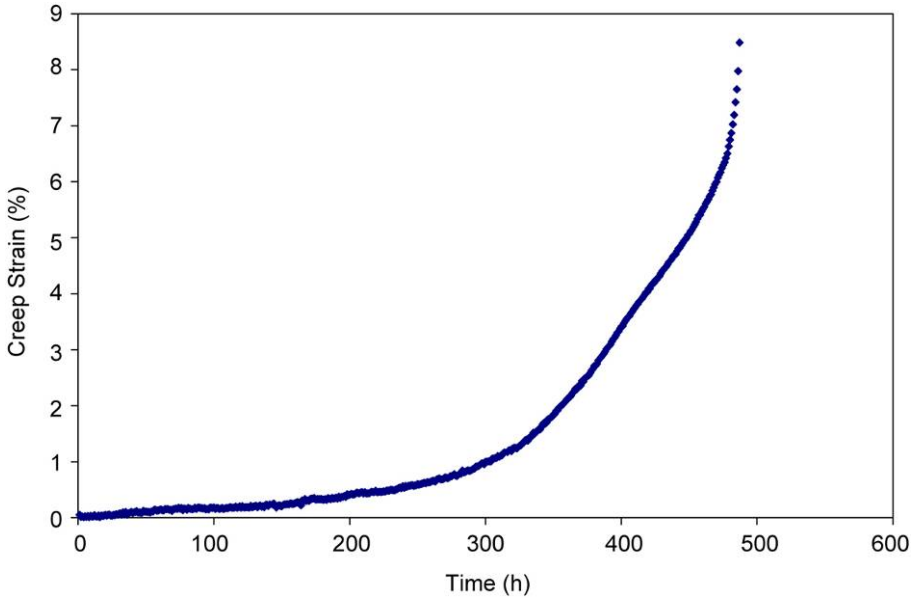

Fig. 4.27. Creep strain as a function of time obtained for commercial alloy Supertherm during testing at 2200°F (1204°C) and 500 psi. Time to rupture was 477 h.

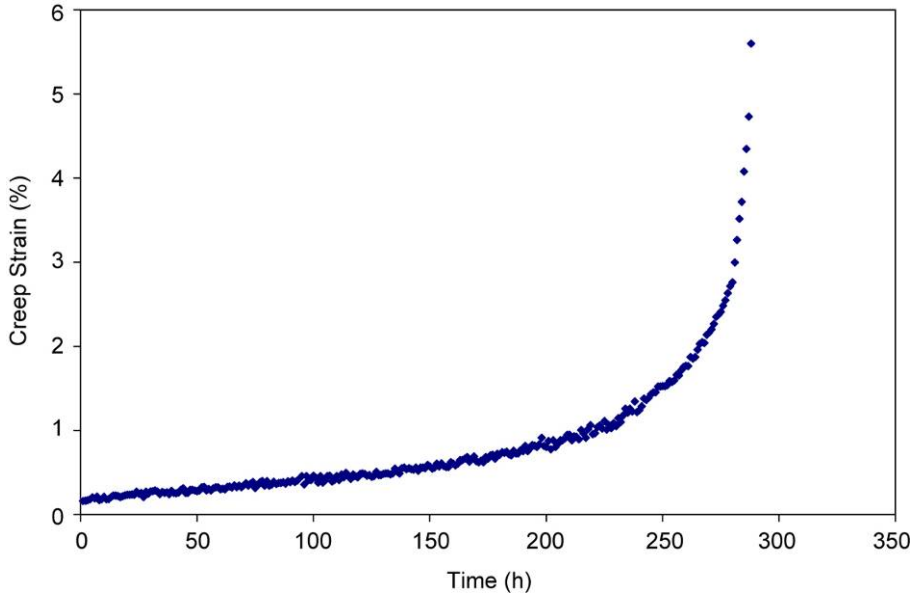

Fig. 4.28. Creep strain as a function of time obtained for alloy S-22H during testing at 2200°F (1204°C) and 500 psi. Time to rupture was 289 h.

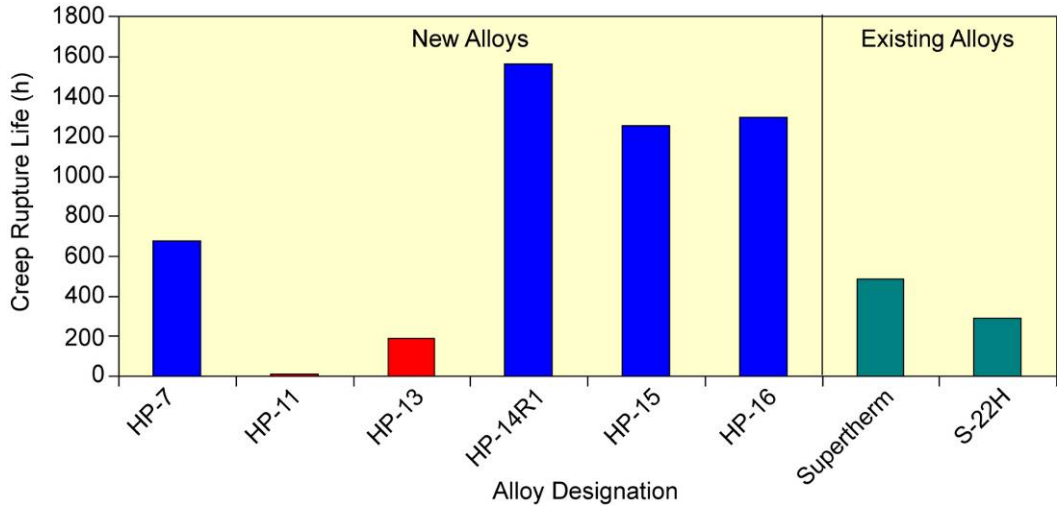

Fig. 4.29. Additions of alloying elements to HP-11 results in new alloys with improved creep rupture life at 2200°F (1204°C) and 500 psi. Times to rupture for some of the new alloys are better than existing alloys.

Table 4.7. Summary of alloys tested, creep testing conditions, and time to rupture under different testing conditions

Alloy designation	1800°F, 4 ksi	2000°F, 1 ksi	2000°F, 2000 psi	2000°F, 2400 psi	2100°F, 1 ksi	2200°F, 100 psi
HP-1	762	1496	204	63	-	274
HP-2	608	825	118	58	-	233
HP-3	746	-	404	-	-	-
HP-4	984	-	291	-	-	-
HP-5	650	-	401	-	-	-
HP-6	979	-	584	-	-	450
HP-7	1497	-	1401	-	-	675
HP-10	770	-		-	427	388
HP-11	922	-	546	-	-	14
HP-12	-	-	20	-	-	5
HP-13	67	-	43	-	-	189
HP-14		-	207	-	-	-
HP-14R1	576	-		-	-	1558
HP-14R2		-	130	-	-	-
HP-15	102	-	139	-	-	1251
HP-16		-	338	-	-	1293
HP-16C	585	-	-	-	-	477
SUPERTHERM	971	-	-	-	-	488
MORE 2	-	-	-	-	-	3147
S-22H	-	-	-	-	-	289
HK-3	-	-	460	-	-	831
HK-4	327	-	196	-	-	526
HK-6	-	-	509	-	-	267

4.3.3 Thermodynamic Calculations and Creep Properties of New HK-Type Alloys

An approach similar to that used for the development of new HP alloys was used for the development of new HK-alloys. Figure 4.30(a) shows the results of thermodynamic calculations, and 4.30(b) shows the creep curve obtained from an alloy HK-3 developed at ORNL. Figure 4.31 compares the creep rupture life of two HK-alloys developed at ORNL with a commercially available HP-type alloy. The properties of the two HK alloys are better than an HP alloy at the test temperature of 2200°F (1204°C).

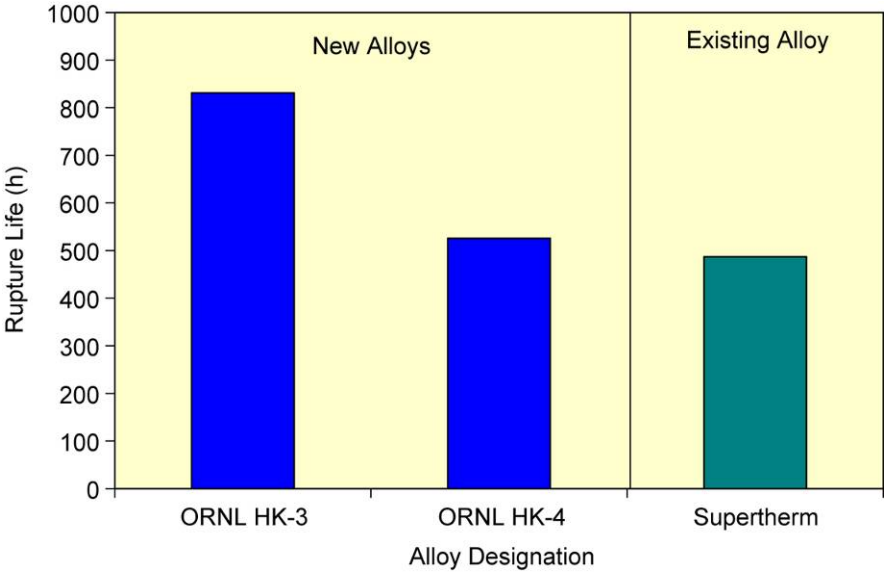

Fig. 4.30. Thermodynamic calculations and creeps strain measurements for HK-3: (a) thermodynamic calculations; (b) creep strain as a function of time obtained during testing at 2200°F (1204°C) and 500 psi.

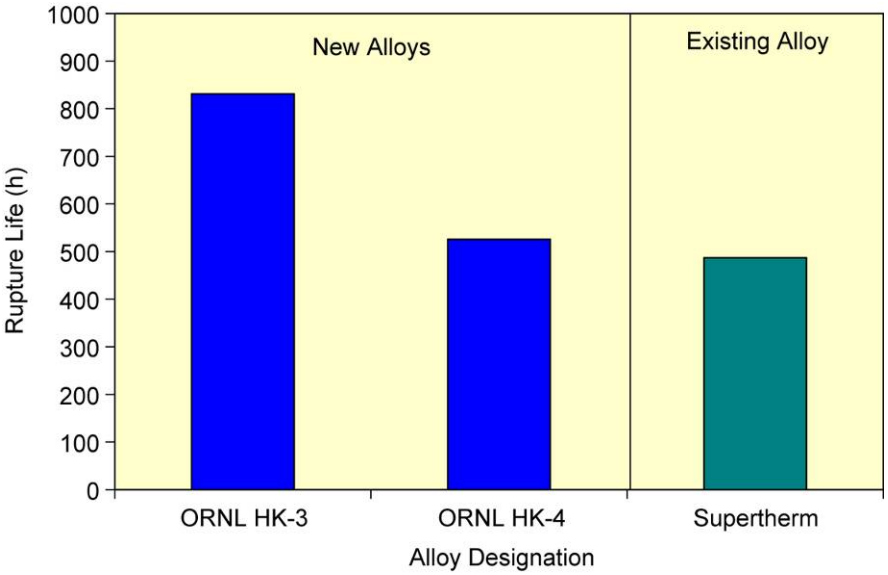

Fig. 4.31. New HK alloys with improved creep rupture life at 2200°F (1204°C) and 500 psi are comparable to Supertherm, a commercial HP-type alloy.

4.3.4 Application of New Alloys in Industrial Use

Radiant burner tube assemblies of the newly developed HP grades were produced by Duraloy Technologies and installed at Nucor Steel. Figure 4.32 shows a typical radiant tube assembly. Tubes have operated successfully for more than a year in a steel reheating furnace. Based on this experience, Nucor has ordered additional radiant burner tube assemblies.

Figure 4.33 shows a furnace roll cast at Duraloy from an HK alloy developed in this project.

Fig. 4.32. Typical radiant-tube assembly fabricated using newly developed HP alloys.

Fig. 4.33. Furnace roll cast at Duraloy Technologies from HK alloy developed in this project.

5. Accomplishments

This project has accomplished the technical, technology transfer, and commercialization goals described below.

5.1 Technical Goals

The two major goals for this project were (1) to increase the creep strength of current HK and HP steels by 50% and (2) to increase their upper use temperature limit by 86–140°F (30–60°C). Both of the goals were achieved during this project. The following were the specific accomplishments of this project:

- Developed a computational method for designing high-strength, low-cost versions of the standard grades of cast austenitic stainless steels known as HK and HP steels.
- Validated a computational method for predicting phases in the HK and HP steels by microstructural analysis.
- Used the validated computational method to develop new compositions of HK and HP steels. Two patents have been filed for the newly developed compositions.
- Validated creep data on newly designed compositions of both HK and HP steels at a test temperature of 2200°F (1204°C) and a stress of 500 psi.
- Melted the newly designed alloys with validated creep performance and cast these materials into tubes at Duraloy.
- Fabricated the new HP alloy tubes into radiant burner tubes, which have been in operation at Nucor Steel for nearly 12 months.
- Ensured that the project met the proposed goals of extending the upper use temperature by 86–140°F (30–60°C).
- Established that the energy savings for the applications identified thus far would be ~15.6 trillion Btu/year by 2015 to 2020. Higher energy savings will result as new applications are implemented.
- Projected that the outcome from the proposed project has given the United States a new lead in higher-strength H-Series stainless steels with very significant energy and associated cost savings.

5.2 Technology Transfer

The makeup of the project team led by Duraloy Technologies, an alloy and component producer, made the technology transfer process easier. Many of the users were partners on the project and have become familiar with the new technology through review meetings and visits to their plants by the Duraloy staff. It is through these efforts that Nucor Steel has been testing the radiant burner tube assemblies of the newly developed HP steel in its plant. Many of the mini-steel mills have shown great interest in using the new steels in their steel reheating furnaces.

Two alloys have been successfully commercialized:

- The HK alloy that met the project goal has been designated by Duraloy as TMA® 4701. Its nominal composition consists of Fe-25Ni-25Cr-0.7Mn-1.5Si-0.6C-0.2Mo-0.5W-0.3Nb.
- The HP alloy that met the project goal has been designated by Duraloy as TMA® 6301. Its nominal composition consists of Fe-34Ni-23Cr-1Mn-0.7Si-0.4C-0.5Mo-0.1W-0.3Nb.

Two patent applications have been filed. Duraloy will use the patents for their core business and will license the technology for other applications. Some initial licensing inquiries have already been received.

In addition, this project has been nominated for an R&D 100 Award for 2006.

The technology transfer of the results from this project is considered a success.

5.3 Publications and Patents

Publications and presentations from this project are listed below.

1. G. Muralidharan, N. D. Evans, K. C. Liu, J. G. Hemrick, M. L. Santella, P. J. Maziasz, and R. I. Pankiw, "Effect of Precipitation on Creep Properties of Certain Cast H-Series Austenitic Stainless Steels," *Proceedings of Materials Science & Technology 2004,* pp. 651–661.
2. G. Muralidharan, N. D. Evans, K. C. Liu, J. G. Hemrick, M. L. Santella, P. J. Maziasz, and R. I. Pankiw, "Development of Stronger and More Reliable Cast Austenitic Stainless Steels (H-Series) Based on a Scientific Design Methodology," *Materials Science & Technology 2004*, 2004 ASM Materials Solutions Conference and Exposition, Columbus, Ohio, October 18–20, 2004.
3. G. Muralidharan, N. D. Evans, K. C. Liu, J. G. Hemrick, M. L. Santella, P. J. Maziasz, V. K. Sikka, and R. I. Pankiw, "Precipitation and Its Effect on the Creep Properties of Certain Cast H-Series Austenitic Stainless Steels," pp. 443–448 in *Solid-to-Solid Phase Transformations in Inorganic Materials 2005,* vol. 1, *Diffusional Transformations,* ed. J. M. Howe et al., TMS (2005).

In addition to publications and presentations, the following two patent disclosures were submitted from this project:

1. G. Muralidharan, V. K. Sikka, P. J. Maziasz, and R. I. Pankiw, "Low-Cost, Cast, Heat-Resistant Austenitic Stainless Steel Compositions having Improved High-Temperature Creep Properties," ID 1445C, S-105,041, submitted to U.S. Patent Office on August 27, 2004.
2. G. Muralidharan, V. K. Sikka, P. J. Maziasz, and R. I. Pankiw, "Cast Heat-Resistant Austenitic Stainless Steels with Improved High Temperature Creep Properties and Balanced Alloying Element Additions (Rev. 1)," ID 1300001544, S-105-146, submitted to UT/Battelle in April 2005.

5.4 Commercialization

The progress made toward the commercialization included the following:

1. A data sheet comparing creep properties of newly developed HK and HP grades with currently used alloys was prepared and sent to the industrial users of HK and HP grades.

2. Radiant burner tube assemblies of the newly developed HP grades were produced and installed at Nucor Steel. The tubes have operated successfully for nearly 12 months. Based on this experience, Nucor has ordered additional radiant burner tube assemblies.
3. Based on the data sheet, Nucor plants in Indiana and Alabama have shown a strong interest in installing uncooled rolls in their thin-slab reheating furnaces to replace water-cooled rolls. Similar interest has been shown by Steel Dynamics. A proposal requesting DOE funding for uncooled roll application for the new HP grades was submitted to DOE-ITP in October 2005.
4. Air Products has shown a strong interest in using the new high-strength HP grade for furnace tubes in its hydrogen cracking furnace.
5. Duraloy has successfully produced in an industrial setting tubes (~4 in. OD × 8 ft) of the new HK alloy developed in this project. Testing is being performed on these tubes, and discussions are being held with possible user companies.
6. Discussions are under way with other industrial customers for many other applications.

Because Duraloy is a commercial producer of HK and HP grades, it is relatively easy for the company to introduce the newly developed grades to industrial customers as higher-performance materials.

The newly developed grades of HK and HP are no more expensive than the standard grades. Furthermore, these new alloys have strength and creep properties exceeding those of Supertherm and are free of expensive cobalt additions. In addition, the weldability of the newly developed grades is similar to that of the currently used grades; the new alloys also have higher creep strength values.

6. Summary and Conclusions

6.1 Summary

The research and development work for this project was conducted by a team consisting of Duraloy Technologies, ISG, The Timken Company, Energy Industries of Ohio, Harper International, IPSCO, Nucor Steel, and ORNL.

The project focused on developing and utilizing a computational method for identifying new cast austenitic steel compositions with 50% higher creep strength and an upper use temperature extended by 86–140°F (30–60°C) over commonly used HK and HP grades. The computational method used thermodynamic modeling to predict the volume percentage of phases and their stability as a function of temperature. The predicted volume percentage was validated through detailed microstructural analysis. The creep rupture strength data for a range of alloys were correlated with the phase volume percentages. These correlations were used as a guide to design new alloy compositions that would meet the project goals of higher strength and increasing the upper use temperature. The computational method allowed the design of new alloys using lower cost elements.

The newly designed alloys were melted into 25- to 50-lb heats and cast into slab. Test bars from experimental heats were creep-tested at 2200°F (1204°C), with some tests performed at lower temperatures; one test was done at 2300°F (1260°C). The experimental alloys that met the project objective were melted in large quantities at Duraloy Technologies and cast into tubes. The cast tubes were fabricated into radiant burner tube assemblies, which have been in testing at Nucor Steel for nearly 12 months.

The new alloy compositions have been introduced to steel and chemical industries for other applications, including uncooled rolls for steel reheating furnaces and tubes for steam hydrogen cracking furnaces. Two patent applications were prepared on the new compositions.

6.2 Conclusions

The following are the important accomplishments of this project:

- The combination of computational thermodynamic modeling with experimental validation is a powerful new approach that enables much shorter alloy design times.
- The use of a project team consisting of materials suppliers, industrial user companies, and a national laboratory can lead to more rapid implementation of research and development results and the replication of these results across industry.
- Development of new structural materials can lead to higher energy efficiencies for a variety of industrial processes.
- Development of intellectual property is an important element in the successful implementation, replication, and use of a new materials technology by the industrial partners.

6.3 Commercialization Aspects: Plans, Status, and Barriers

Because project partner Duraloy is a materials and component supplier, it is relatively easy for the company to introduce the newly developed steels to customers as higher-performance materials. Other aspects of the commercialization plan and status for these new alloys include the following:

1. Several potential users of the cast austenitic stainless steels are partners in the project and, thus, have been briefed on the new advances made during this project. This creates a user demand for these higher strength materials. For example, two Nucor Steel plants as well as Steel Dynamics are requesting the use of new materials for uncooled rolls in steel reheating furnaces.
2. User partners are already installing radiant burner tubes from the new alloys in their production plants, and assembly lines using the new alloys have operated successfully for nearly 12 months. Such success will encourage other companies to use new materials for their applications.
3. Broad-based dissemination of information about these alloys was planned by presenting papers at national technical meetings. Three papers were presented at national technical meetings.
4. A comparative data sheet for customer information has been prepared. More data are needed to prepare a comprehensive data sheet.

The following are the barriers for a broad-based acceptance for new grades:

1. More creep data are needed over a broader test temperature range. This project focused only on data at 2200°F (1204°C).
2. Creep data are needed for test times exceeding 10,000 h. Data were recorded during this project only for test times up to approximately 2000 h.
3. Although the new grades weld similar to standard grades, in order to take full advantage of higher base metal strength, additional development is needed in weld filler wire compositions with strength matching the base metal.

7. Recommendations

This project has accomplished all the tasks that were proposed. The following activities would build upon and extend the information already obtained in the project:

1. Creep data are the limiting factors in use of these steel alloys for very-high-temperature applications. Creep data are needed in the test temperature range of 1650 to 2200°F (900 to 1204°C) and for test times exceeding 10,000 h. These data are needed for three to five different heats of a specified composition. Duraloy is currently performing creep tests in a defined temperature range to complete the alloy design database. However, additional data are also needed.
2. This project has developed higher-strength versions of HK and HP steels. However, these new alloys will still be welded by the lower-strength weld filler wire. The computational approach developed for the base metal in this project should also be extended to develop new weld filler compositions that match or exceed the base metal compositions.
3. For some high-risk applications such as replacing water-cooled rolls with uncooled rolls, there is a need for DOE funding to minimize the use risk. However, if successful, use of these new alloys in such applications has the potential to increase energy savings.
4. No corrosion data were developed for the newly developed steels in this project. There is a great need for generating data in oxidizing, carburizing, and sulfidizing environments.

8. References

1. E. A. Schoefer, “Seventy-Five Years of Cast High Alloys,” pp. 3–10 in *Stainless Steel Castings*, ASTP STP 756, ed. V. G. Behal and A. S. Melilli, American Society for Testing and Materials, Philadelphia, Pa. (1982).
2. C. M. Schillmoller, “Alloy for Ethylene Cracking Furnace Tubes,” pp. 469–476 in *Heat-Resistant Materials*, ed. K. Natesan and D. J. Tillack, ASM-International, Materials Park, Ohio (1991).
3. T. Yoshimoto and M. Takahashi, “New Heat Resistant Cast Alloys and Non-Destructive Inspection Techniques in the Petrochemical Industry,” pp. 461–468 in *Heat-Resistant Materials*, ed. K. Natesan and D. J. Tillack, ASM-International, Materials Park, Ohio (1991).
4. M. C. Blair, “Cast Stainless Steels,” pp. 908–929 in *Metals Handbook—Properties and Selection: Irons, Steels, and High-Performance Alloys*, Vol. 1, 10th ed., ASM-International, Materials Park, Ohio (1990).
5. P. J. Maziasz, “Developing an Austenitic Stainless Steel for Improved Performance in Advanced Fossil Power Facilities,” *Journal of Metals*, **41,** 14–20 (July 1989).
6. P. J. Maziasz, “Microstructural Stability and Control for Improved Irradiation Resistance and for High-Temperature Strength of Austenitic Stainless Steels,” pp. 116–161 in *MiCon ’86: Optimization of Processing, Properties and Service Performance Through Microstructural Control*, ASTM STP 979, ed. B. L. Bramfitt, R. L. Benn, C. R. Brinkman, and G. F. Vander Voort, American Society for Testing and Materials, Philadelphia, Pa. (1988).
7. R. W. Swindeman and P. J. Maziasz, “The Mechanical and Microstructural Stability of Austenitic Stainless Steels Strengthened by MC-Forming Elements,” pp. 33–42 in *Creep: Characterization, Damage and Life Assessment*, ASM-International, Materials Park, Ohio (1992).
8. R. W. Swindeman and P. J. Maziasz, “The Effect of MC Forming Additions and 10% Cold Work on the High Temperature Strength of 20Cr-30Ni-Fe Alloys,” pp. 251–259 in *Heat-Resistant Materials*, ed. K. Natesan and D. J. Tillack, ASM-International, Materials Park, Ohio (1991).
9. M. A. Harper, G. D. Smith, P. J. Maziasz, and R. W. Swindeman, “Selecting and Developing Advanced Alloys for Creep-Resistance for Microturbine Recuperator Applications,” Proceedings of ASME Turbo Expo 2001, June 4–7, 2001, New Orleans, La.
10. P. J. Maziasz, R. W. Swindeman, M. T. Kiser, C. W. Siebenaler, and M. E. Frary, “Development of Low-Cost Austenitic Stainless Diesel Engine Components with Enhanced High-Temperature Reliability,” *DOE Office of Transportation Technology Heavy Vehicle Propulsion Materials Program Quarterly Progress Report*, Period Ending March 31, 2001.
11. P. J. Maziasz and M. J. Pollard, “High-Temperature Cast Stainless Steel,” *Advanced Materials and Processes,* **161**(10), 57–59 (2003).
12. Q. Chen and B. Sundman, *TQ-1 Thermodynamic Calculation Interface: Programmers’ Guide and Examples*, Thermo-Calc Software AB, Stockholm (1999).
13. A. Jansson and B. Sundman, “Simulation of Solidification of Light Alloys Using a Thermodynamic Database (1997),” in A. Jansson, “Phase Diagram Evaluation and Applications in Light Metal Alloys,’ KTH Ph.D. diss., Royal Institute of Technology (KTH), Stockholm.
14. N. Saunders, “Phase Diagram Calculations for Commercial Al-Alloys,” 5th International Conference on Aluminum Alloys, Their Physical and Mechanical Properties, July 1996, Grenoble, France.
15. B. Sundman, B. Jansson, and M. Schalin, “Thermodynamic Calculations Made Easy,” *Journal of Phase Equilibria*, 573–562 (1993).

16. E. Scheil, "Bemerkungen zur schichtkristallbildung," *Zeitschrift für Metalkunde*, **34**, 70–72 (1942).
17. G. Muralidharan, N. D. Evans, K. C. Liu, J. G. Hemrick, M. L. Santella, P. J. Maziasz, and R. I. Pankiw, "Effect of Precipitation on Creep Properties of Certain Cast H-Series Austenitic Stainless Steels," *Proceedings of Materials Science & Technology 2004*, pp. 651–661.
18. G. Muralidharan, N. D. Evans, K. C. Liu, J. G. Hemrick, M. L. Santella, P. J. Maziasz, V. K. Sikka, and R. I. Pankiw, "Precipitation and Its Effect on the Creep Properties of Certain Cast H-Series Austenitic Stainless Steels," Proceedings of the Conference on Solid-Solid Phase Transformations in Inorganic Materials 2005, May 29–June 3, 2005, Phoenix, AZ.